So far, we discussed static instability (vertical acceleration) through parcel theory

$$\frac{dw}{dt} = B,$$

上节课回顾

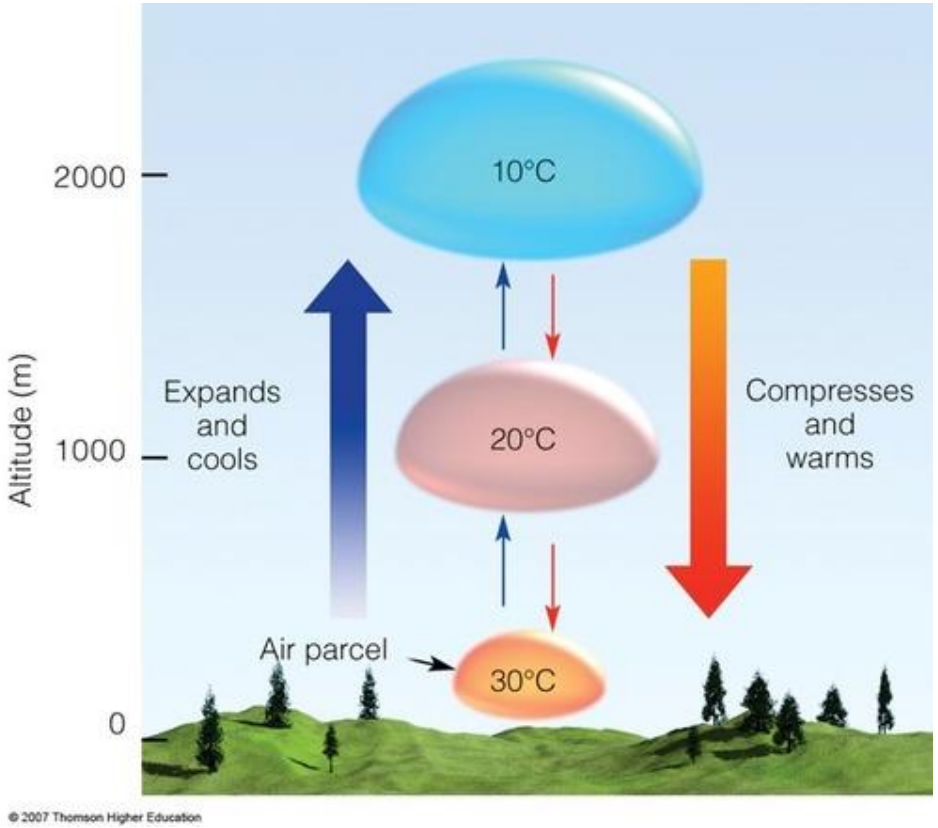

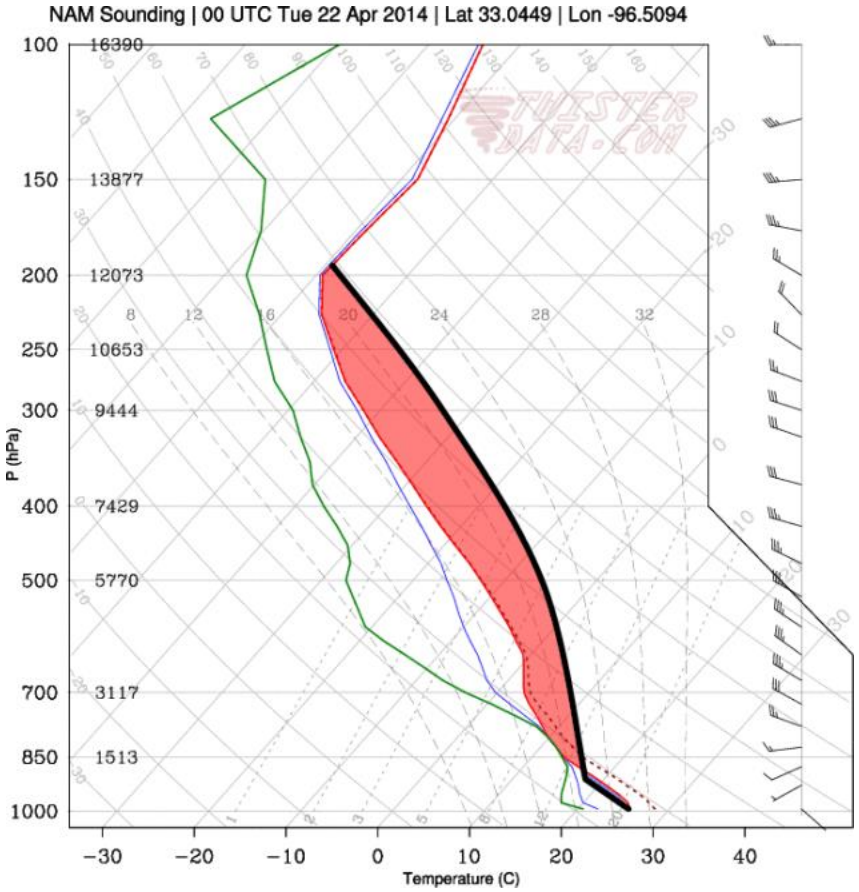

Neglecting the following

1) pressure perturbation
2) entrainment
3) hydrometeors
4) subsidence

上节课回顾

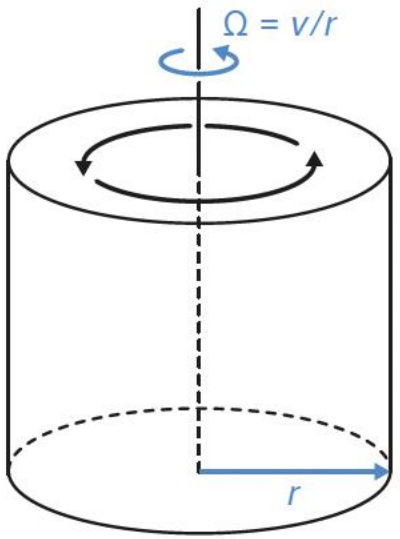

Figure 3.4 A cylindrical tank of spinning fluid, spinning at an angular velocity of $\Omega = v/r$.

The equations of horizontal motion in cylindrical coordinates are

$$\frac{\mathrm{d}u}{\mathrm{d}t} = -\alpha_0 \frac{\partial p}{\partial r} + \frac{v^2}{r} \tag{3.19}$$

$$\frac{\mathrm{d}(vr)}{\mathrm{d}t} = -\alpha_0 \frac{\partial p}{\partial \theta} \tag{3.20}$$

If we assume pressure field is symmetric,

$$\frac{\mathrm{d}u}{\mathrm{d}t} = -\alpha_0 \frac{\partial p}{\partial r} + \frac{M^2}{r^3} \tag{3.21}$$

$$\frac{\mathrm{d}M}{\mathrm{d}t} = 0. \tag{3.22}$$

the angular momentum $M = vr$,

Let us define a mean state and consider its perturbations

上节课回顾

Let us define a mean state such that no radial acceleration exists and the horizontal pressure gradient force and centrifugal force balance each other:

$$0 = -\alpha_0 \frac{\partial \overline{p}}{\partial r} + \frac{\overline{M}^2}{r^3}. \tag{3.23}$$

Subtracting (3.24) from (3.22) gives

$$\frac{\mathrm{d}u}{\mathrm{d}t} = -\alpha_0 \frac{\partial p'}{\partial r} + \frac{1}{r^3}(M^2 - \overline{M}^2), \tag{3.24}$$

where $p = \overline{p} + p'$ and $M = \overline{M} + M'$. If we neglect the effects of the perturbation pressure gradient, as is done in parcel theory, we obtain

$$\frac{\mathrm{d}u}{\mathrm{d}t} = \frac{1}{r^3}(M^2 - \overline{M}^2). \tag{3.25}$$

The square of the mean angular momentum at the location of the displaced ring is (using a first-order Taylor series approximation)

$$\overline{M}^2 = M_0^2 + \frac{\mathrm{d}\overline{M}^2}{\mathrm{d}r}\Delta r, \tag{3.26}$$

where M_0 is the value of $\overline{M}$ at $r = r_0$. Also, because M^2 is conserved, its value for parcels within the displaced ring is

$$M^2 = M_0^2; \tag{3.27}$$

that is, a ring of fluid in equilibrium at r_0 retains its M^2 when displaced to $r_0 + \Delta r$. Therefore, for small Δr, and noting that $\mathrm{d}u/\mathrm{d}t = \mathrm{d}(\mathrm{d}r/\mathrm{d}t)/\mathrm{d}t = \mathrm{d}^2\Delta r/\mathrm{d}t^2$, (3.25) becomes

$$\frac{\mathrm{d}^2\Delta r}{\mathrm{d}t^2} = \frac{M^2 - \overline{M}^2}{(r_0 + \Delta r)^3} \tag{3.28}$$

$$\approx \frac{M_0^2 - \left(M_0^2 + \dfrac{\mathrm{d}\overline{M}^2}{\mathrm{d}r}\Delta r\right)}{r_0^3} \tag{3.29}$$

$$= -\frac{1}{r_0^3}\frac{\mathrm{d}\overline{M}^2}{\mathrm{d}r}\Delta r. \tag{3.30}$$

The general solution of (3.31) is

$$\Delta r(t) = C_1 \mathrm{e}^{i\left[\frac{1}{r_0^3}\frac{\mathrm{d}\overline{M}^2}{\mathrm{d}r}\right]^{1/2} t} + C_2 \mathrm{e}^{-i\left[\frac{1}{r_0^3}\frac{\mathrm{d}\overline{M}^2}{\mathrm{d}r}\right]^{1/2} t}, \tag{3.31}$$

上节课回顾

Let us consider the simple case of a zonal geostrophic wind that varies in the north-south (y) direction, that is, $u_g = u_g(y)$ and $v_g = 0$. Using a similar methodology as for the centrifugal stability analysis, we start with the horizontal equations of motion in Cartesian coordinates. In this case, they can be written as

$$\frac{du}{dt} = fv \tag{3.32}$$

$$\frac{dv}{dt} = f(u_g - u). \tag{3.33}$$

The variables u and v are the actual velocity components, which may include an ageostrophic component.

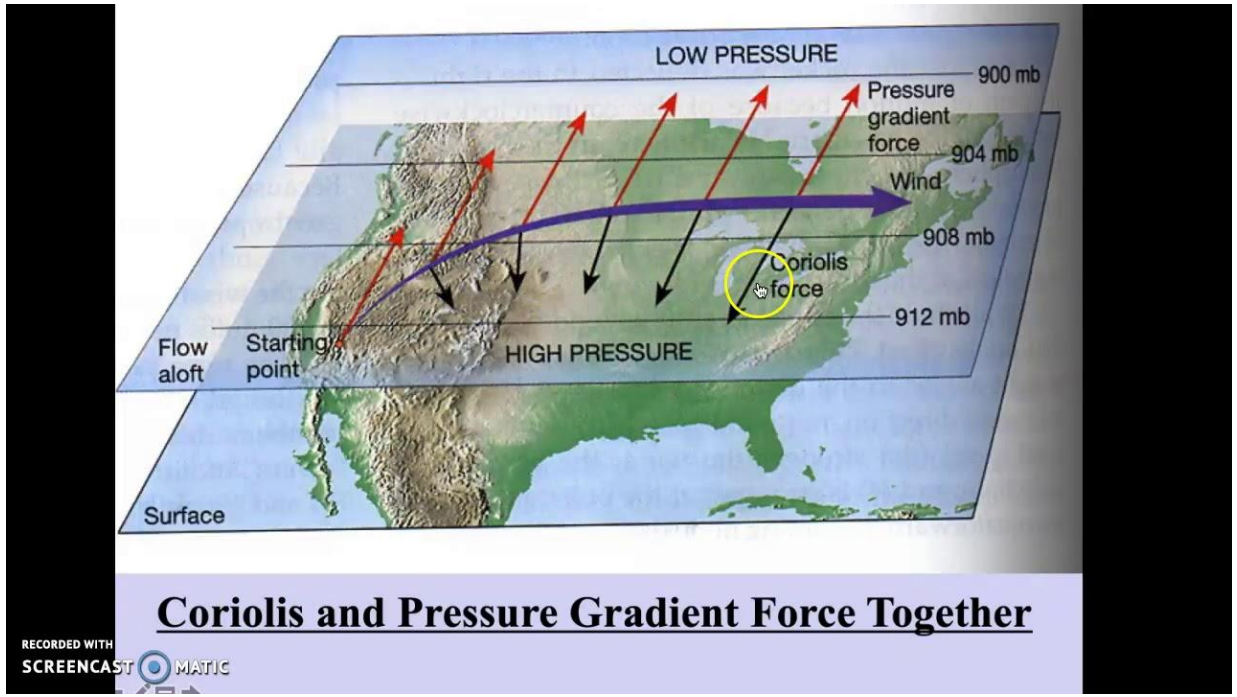

上节课回顾

$$\frac{du}{dt} = fv \tag{3.32}$$

$$\frac{dv}{dt} = f(u_g - u). \tag{3.33}$$

The variables u and v are the actual velocity components, which may include an ageostrophic component.

Because $v \equiv dy/dt$, we can rev

$$\frac{du}{dt} = f\frac{dy}{dt} \tag{3.34}$$

$$\frac{d^2\Delta y}{dt^2} = f(u_g - u), \tag{3.35}$$

where Δy is the horizontal displacement distance from the initial position (i.e., $y = y_0 + \Delta y$ at some future time; thus, dy/dt can be written as $d\Delta y/dt$).

The term $f - \partial u_g/\partial y$ is the absolute geostrophic vorticity (recall $v_g = 0$, so there is no $\partial v_g/\partial x$ term in the relative vorticity), and the general solution of (3.39) is

$$\Delta y(t) = C_1 e^{i\left[f\left(f-\frac{\partial u_g}{\partial y}\right)\right]^{1/2}t} + C_2 e^{-i\left[f\left(f-\frac{\partial u_g}{\partial y}\right)\right]^{1/2}t}, \tag{3.40}$$

If the tube is displaced northward or southward, the new zonal velocity for a parcel within the tube will be, via integration of (3.34),

$$u = u_0 + f\Delta y. \tag{3.36}$$

Most readers are probably familiar with the above result in that it implies that a parcel moving northward (southward) is accelerated eastward (westward) owing to the
mentum.
e location of the displaced tube
aylor series approximation)

$$+ \frac{\partial u_g}{\partial y}\Delta y. \tag{3.37}$$

initial pressure field and, correspondingly, the geostrophic wind, is not altered by the displacement of the tube. By subtracting (3.36) from the above expression, we obtain

$$u_g - u = \left(\frac{\partial u_g}{\partial y} - f\right)\Delta y, \tag{3.38}$$

and using (3.36), we obtain

$$\frac{d^2\Delta y}{dt^2} + f\left(f - \frac{\partial u_g}{\partial y}\right)\Delta y = 0. \tag{3.39}$$

Symmetric Instability (horizontal acceleration)

上节课回顾

[11] The term *symmetric instability* appears to have originated from studies of centrifugal instability in a rotating tank with baroclinity carried out by H. Solberg (circa 1930). A *symmetric flow* is one in which the base state and perturbations only vary in two dimensions.

Air parcels can be both statically and inertially stable (i.e., in hydrostatic and geostrophic equilibrium, and therefore in thermal wind balance), but can be unstable to displacements along a path that is slanted with respect to the horizontal for certain distributions of geostrophic momentum and potential temperature. This type of instability is called *symmetric instability*.[11] Before embarking on the

上节课回顾

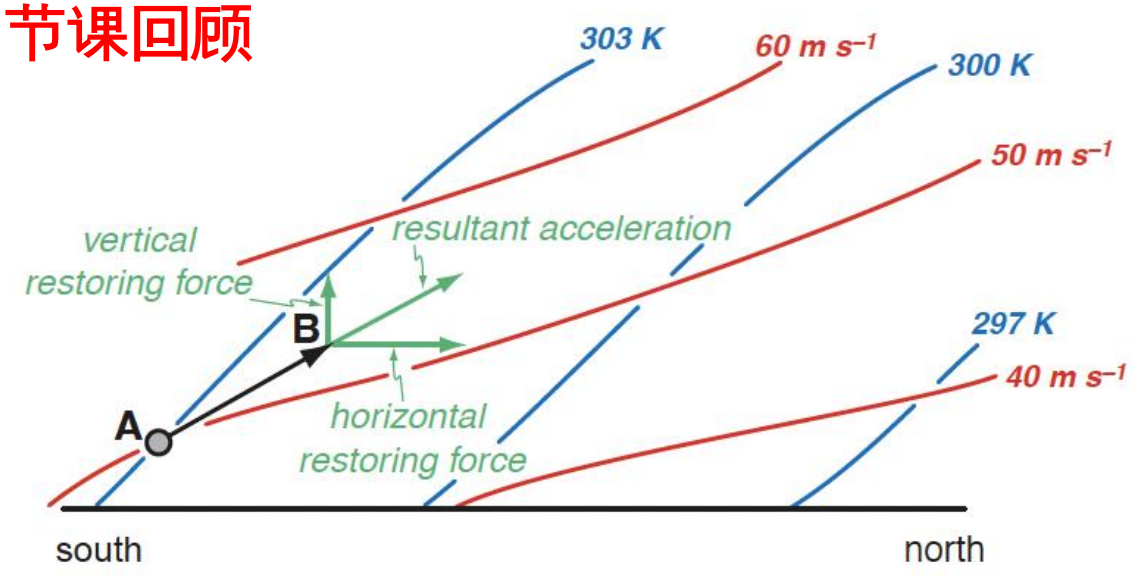

Figure 3.9 Schematic meridional cross-section of isentropic (blue) and geostrophic momentum surfaces (red) in a symmetrically unstable atmosphere. A tube of parcels that is displaced from position A toward position B experiences a resultant acceleration that is directed away from the original equilibrium position.

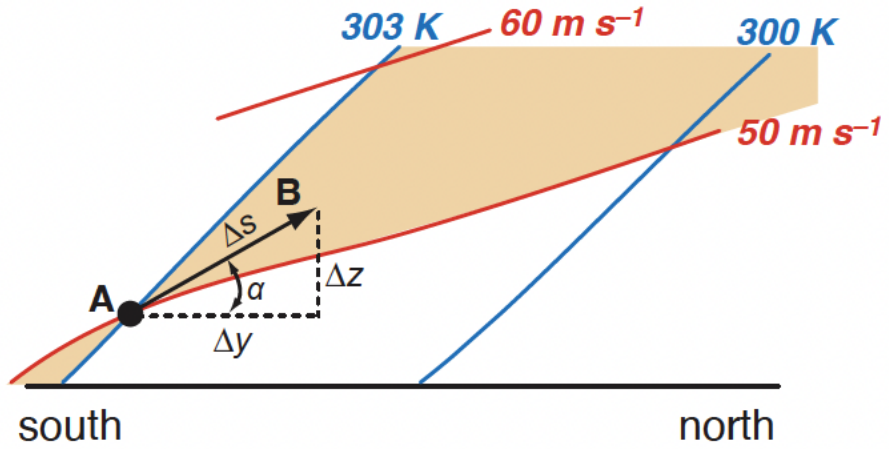

Figure 3.10 Zoomed-in view of Figure 3.9, showing the relationship between α, Δs, Δy, and Δz. Displacements of the parcel at position A to locations within the shaded region (e.g., toward position B) result in acceleration away from position A.

上节课回顾

Barotropic vorticity equation

$$\frac{\partial \zeta}{\partial t} + u\frac{\partial \zeta}{\partial x} + v\frac{\partial \zeta}{\partial y} + v\beta = 0, \qquad (3.68)$$

Linearized version

$$\left(\frac{\partial}{\partial t} + \overline{u}\frac{\partial}{\partial x}\right)\nabla_{\mathrm{h}}^2\Phi' + \frac{\partial \Phi'}{\partial x}\left(\beta - \frac{\partial^2 \overline{u}}{\partial y^2}\right) = 0. \qquad (3.69)$$

Consider a wavelike solution $\Phi' = \hat{\Phi}(y)\mathrm{e}^{ik(x-ct)}$,

Rayleigh equation

$$\frac{\partial^2 \Phi'}{\partial y^2} - k^2\Phi' + \frac{\left(\beta - \frac{\partial^2 \overline{u}}{\partial y^2}\right)}{\overline{u} - c}\Phi' = 0.$$

Necessary condition

$$c_{\mathrm{i}}\int_{-L}^{L} |\Phi'|^2 \frac{\left(\beta - \frac{\partial^2 \overline{u}}{\partial y^2}\right)}{|\overline{u} - c|^2}\mathrm{d}y = 0. \qquad (3.76)$$

上节课回顾

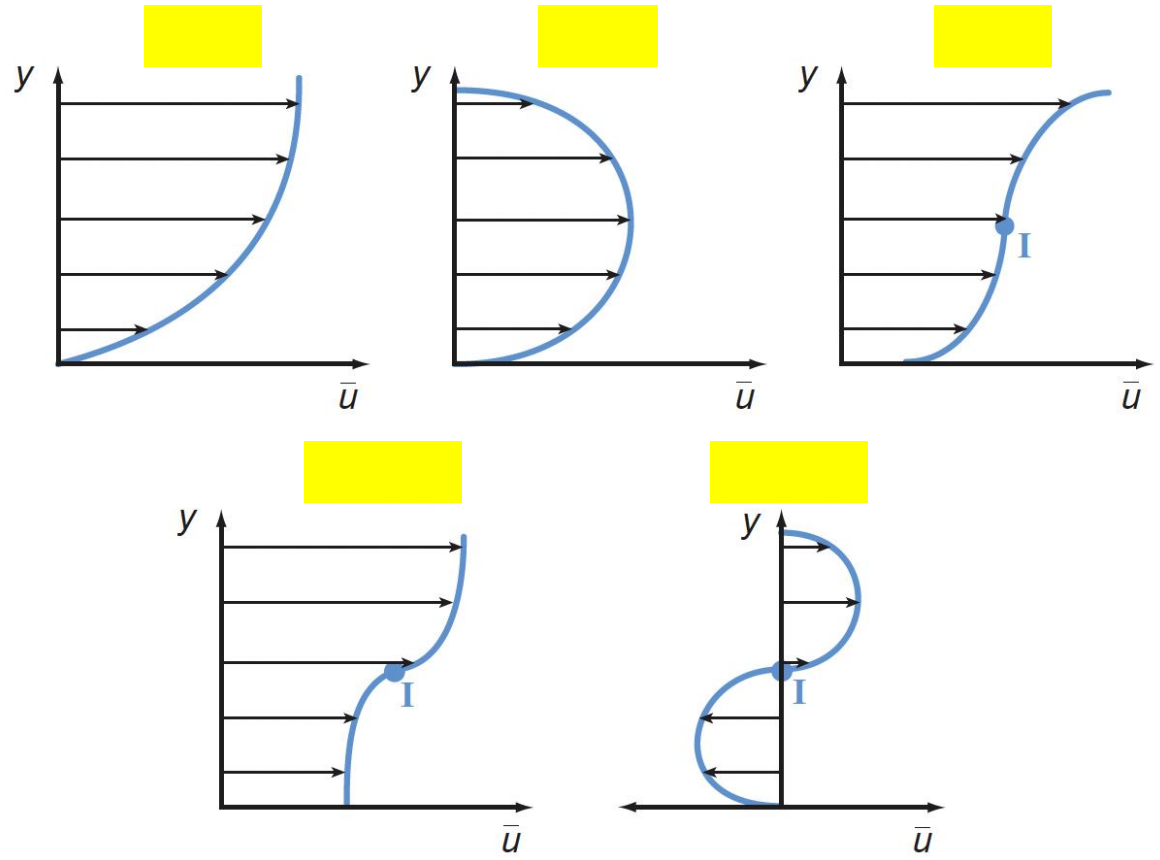

Figure 3.20 Horizontal wind profiles stable and unstable to small perturbations. Inflection points in the wind profiles are denoted with the letter 'I.' (Adapted from Kundu and Cohen [2008].)

Necessary condition

$\beta - \frac{\partial^2 \overline{u}}{\partial y^2}$ changes sign.

More stringent condition

$\frac{\partial^2 \overline{u}}{\partial y^2}(\overline{u} - \overline{u}_I)$ must be less than zero somewhere

$\overline{u}_I$ is the base state zonal wind at the inflection point

Ch2.4 深湿对流的触发

2.7 深湿对流的触发

Deep Moist Convection （DMC）

DMC在何时何地出现？

复杂性：(1) 涉及天气尺度到中尺度的抬升
多尺度天气系统和下垫面复杂的相互作用结果，
具有很强的局地性
（2）中尺度温湿场的不均匀性
（3）天气尺度过程造成的层结变化

DMC常见的发生地点：气团边界，比如锋面、干线
出流边界，海陆锋，地形，重力波等

强对流触发的雷达识别

1) 雷达上首次出现35dBZ回波
2) 该回波发展为强对流

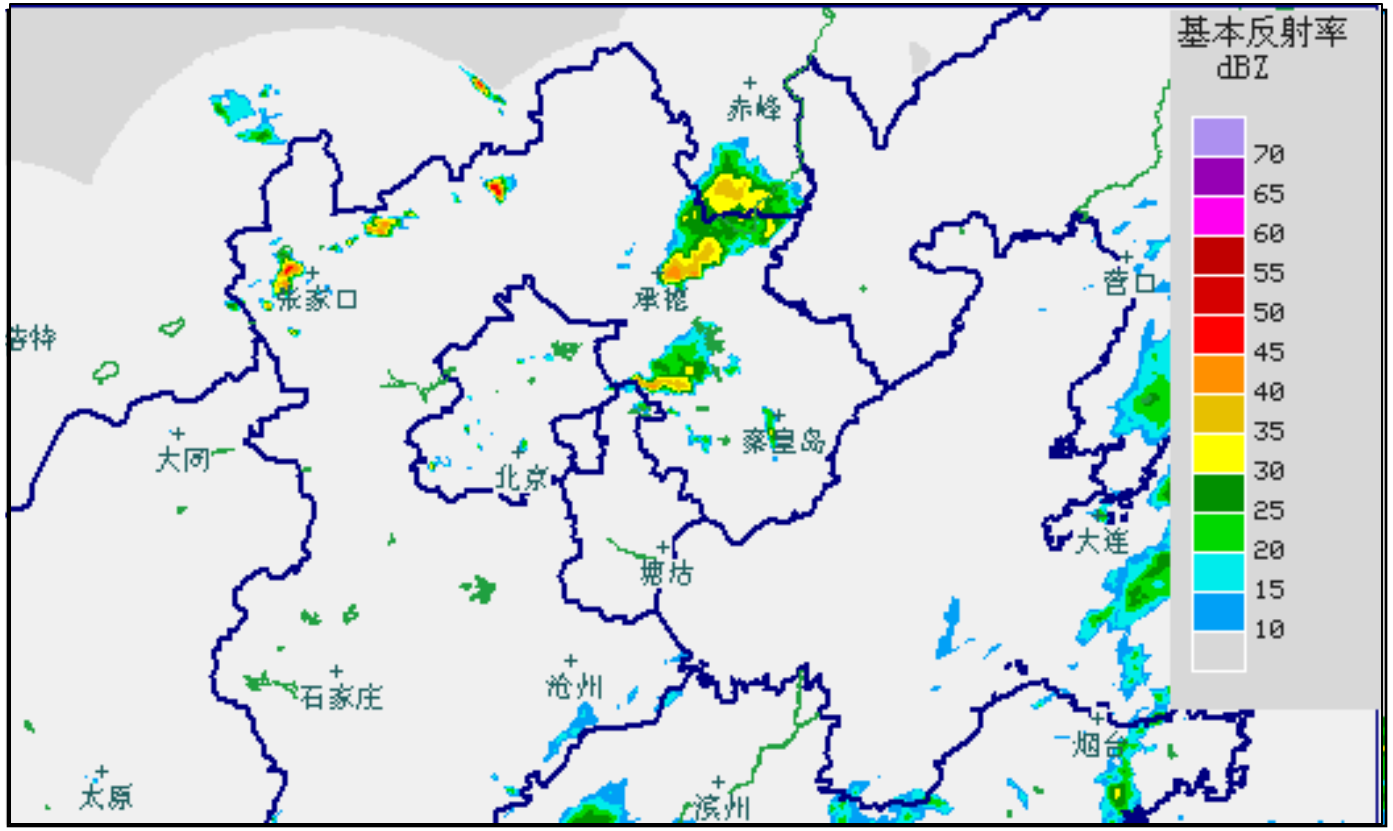

强对流触发的决定性因子

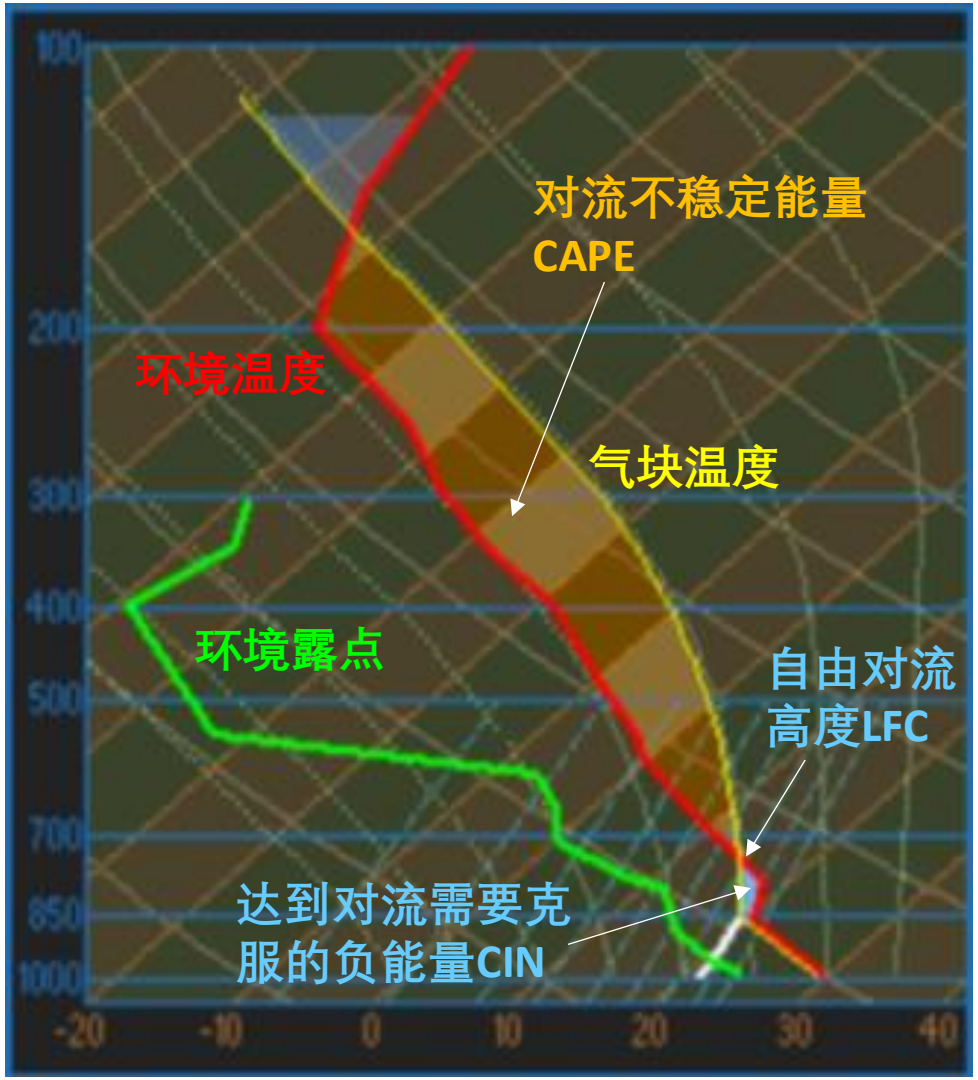

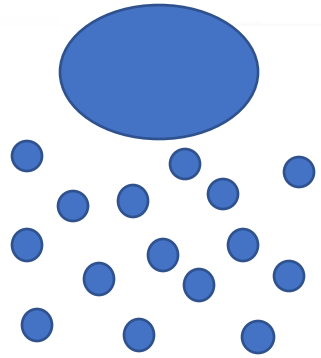

对流触发三大条件：

- **水汽**
- **不稳定能量**
- **抬升机制**

地基对流：地形、边界层辐合线（海陆锋、干线、边界层滚涡、阵风锋）

高架对流：边界层顶附近的抬升

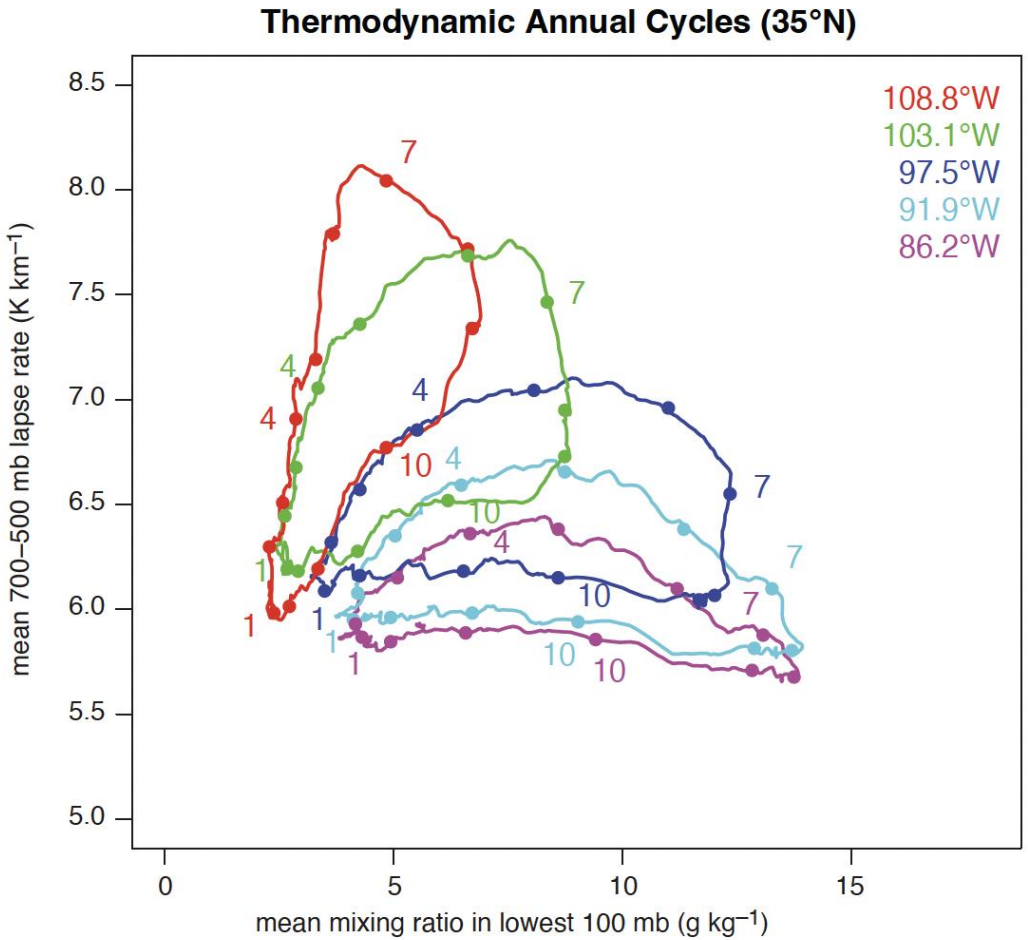

Figure 7.1 Annual cycles of midlevel (700–500 mb) lapse rates versus the mean water vapor mixing ratio in the lowest 100 mb, derived from North American reanalysis data, at five locations in a west-east line located at latitude 35°N, running from approximately northwestern New Mexico (108.8°W) to south central Tennessee (86.2°W). Filled circles along each loop indicate the first day of the month (January, April, July, and October are labeled with the numbers 1, 4, 7, and 10, respectively). CAPE is maximized when rich low-level moisture is overrun by large midlevel lapse rates. This generally occurs in the spring and summer months. Note the differences in the cycles from west to east. The cycles in the western United States are dominated by lapse rate changes from winter to summer, whereas the eastern United States cycles are dominated by moisture changes from winter to summer. Courtesy of Harold Brooks.

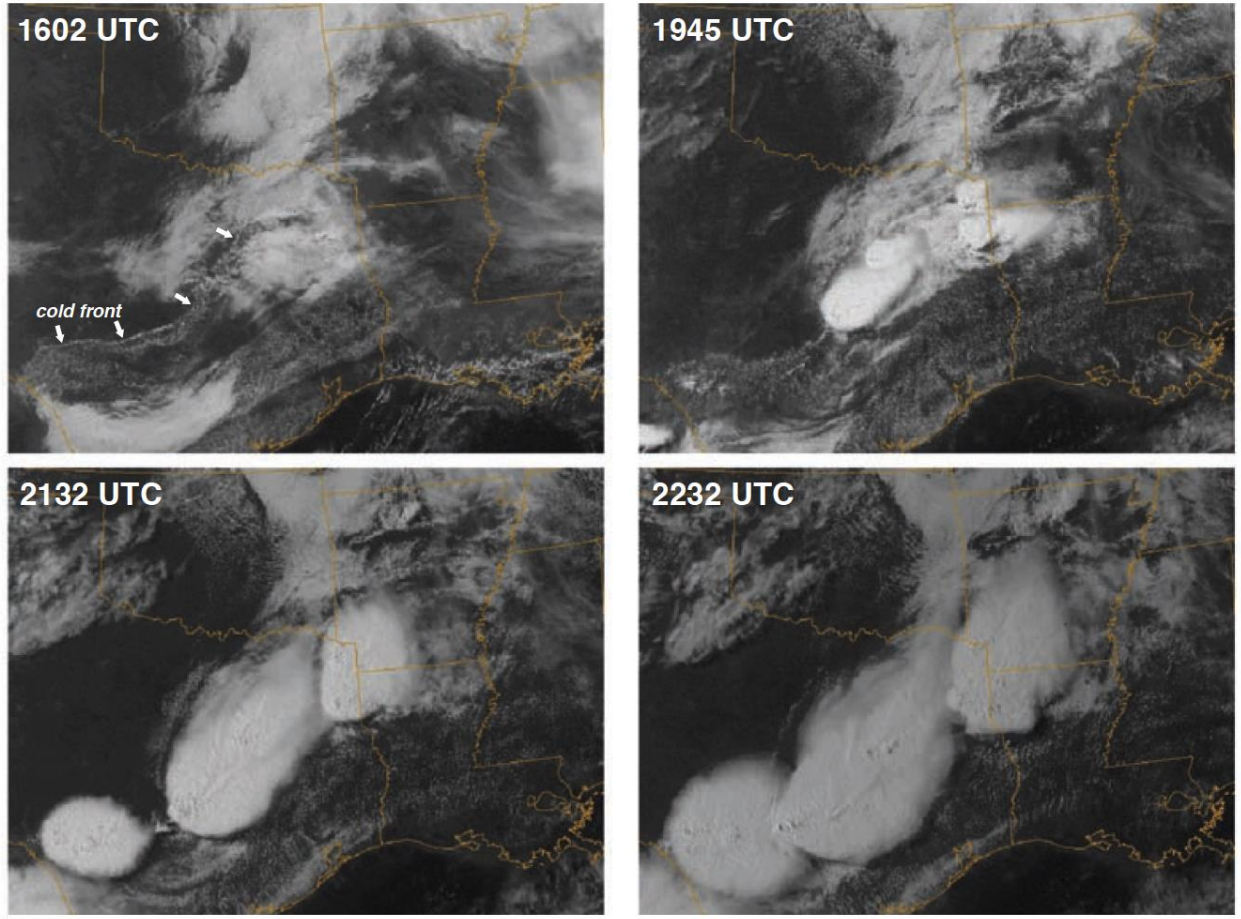

Figure 7.2 In the absence of favored topographic features that act as elevated buoyancy sources, DMC tends to be initiated along air mass boundaries, which are usually accompanied by a wind shift and convergence. This allows forecasters to enjoy at least modest predictability with regard to anticipating the location of convection initiation, for such boundaries are fairly easily observable in routinely available synoptic surface observations and radar and satellite data. The sequence of visible satellite images shows the development of a line of severe thunderstorms along a cold front on 27 May 1997. The town of Jarrell, TX, was devastated by a tornado during this event.

(1）天气尺度系统的作用

Prime the mesoscale environment

-- 减小CIN　-- 加厚低层湿层

1）环境减温率倾向方程 $\frac{\partial \gamma}{\partial t}$

$$c_p \frac{dT}{dt} - \alpha \frac{dp}{dt} = q$$

单位质量气块的加热率

$$\alpha \frac{dp}{dt} = \frac{1}{\rho} \frac{dp}{dz} \frac{dz}{dt} = -\frac{1}{\rho} \rho g \frac{dz}{dt} = -gw$$

$$c_p \left(\frac{\partial T}{\partial t} + \vec{v_h} \cdot \nabla_h T + w \frac{\partial T}{\partial z} \right) + gw = q$$

1）环境减温率倾向方程 $\frac{\partial\gamma}{\partial t}$

$$q = c_p\left(\frac{\partial T}{\partial t} + \vec{v_h}\cdot\nabla_h T + w\frac{\partial T}{\partial z}\right) + gw$$

对上式求 $-\frac{\partial}{\partial z}$

$$-\frac{\partial q}{\partial z} = c_p\left(\frac{\partial\left(-\frac{\partial T}{\partial z}\right)}{\partial t} - \frac{\partial\vec{v_h}}{\partial z}\cdot\nabla_h T + w\frac{\partial\left(-\frac{\partial T}{\partial z}\right)}{\partial z}\right.$$

$$\left. + \vec{v_h}\cdot\nabla_h\left(-\frac{\partial T}{\partial z}\right) + \frac{\partial w}{\partial z}\left(-\frac{\partial T}{\partial z}\right)\right) - g\frac{\partial w}{\partial z}$$

$\gamma = -\frac{\partial T}{\partial z}$

$$-\frac{\partial q}{\partial z} = c_p\left(\frac{\partial\gamma}{\partial t} - \frac{\partial\vec{v_h}}{\partial z}\cdot\nabla_h T + w\frac{\partial\gamma}{\partial z} + \vec{v_h}\cdot\nabla_h\gamma + \frac{\partial w}{\partial z}\gamma\right) - g\frac{\partial w}{\partial z}$$

1）环境减温率倾向方程 $\frac{\partial\gamma}{\partial t}$

$$-\frac{\partial q}{\partial z}=\mathrm{c_p}\left(\frac{\partial\gamma}{\partial t}-\frac{\partial\overrightarrow{\mathbf{v}_\mathrm{h}}}{\partial z}\cdot\nabla_\mathrm{h}T+w\frac{\partial\gamma}{\partial z}+\overrightarrow{\mathbf{v}_\mathrm{h}}\cdot\nabla_\mathrm{h}\gamma+\frac{\partial w}{\partial z}\gamma\right)-\mathrm{g}\frac{\partial w}{\partial z}$$

$$\frac{\partial\gamma}{\partial t}=-\overrightarrow{\mathbf{v}_\mathrm{h}}\cdot\nabla_\mathrm{h}\gamma-w\frac{\partial\gamma}{\partial z}+\frac{\partial\overrightarrow{\mathbf{v}_\mathrm{h}}}{\partial z}\cdot\nabla_\mathrm{h}T-\frac{\partial w}{\partial z}\gamma+\frac{\mathrm{g}}{\mathrm{c_p}}\frac{\partial w}{\partial z}-\frac{1}{\mathrm{c_p}}\frac{\partial q}{\partial z}$$

$$=-\overrightarrow{\mathbf{v}_\mathrm{h}}\cdot\nabla_\mathrm{h}\gamma-w\frac{\partial\gamma}{\partial z}+\frac{\partial\overrightarrow{\mathbf{v}_\mathrm{h}}}{\partial z}\cdot\nabla_\mathrm{h}T+\frac{\partial w}{\partial z}(\Gamma_\mathrm{d}-\gamma)-\frac{1}{\mathrm{c_p}}\frac{\partial q}{\partial z}$$

水平平流　垂直平流　拉伸项　差分非绝热加热

大尺度　10^{-7}　10^{-8}　10^{-8}　10^{-8}　10^{-9}

$$-\overrightarrow{\mathbf{v}_\mathrm{h}}\cdot\nabla_\mathrm{h}\gamma+\frac{\partial\overrightarrow{\mathbf{v}_\mathrm{h}}}{\partial z}\cdot\nabla_\mathrm{h}T=\overrightarrow{\mathbf{v}_\mathrm{h}}\cdot\nabla_\mathrm{h}\left(\frac{\partial T}{\partial z}\right)+\frac{\partial\overrightarrow{\mathbf{v}_\mathrm{h}}}{\partial z}\cdot\nabla_\mathrm{h}T=-\frac{\partial}{\partial z}(-\overrightarrow{\mathbf{v}_\mathrm{h}}\cdot\nabla_\mathrm{h}T)$$

差分温度平流

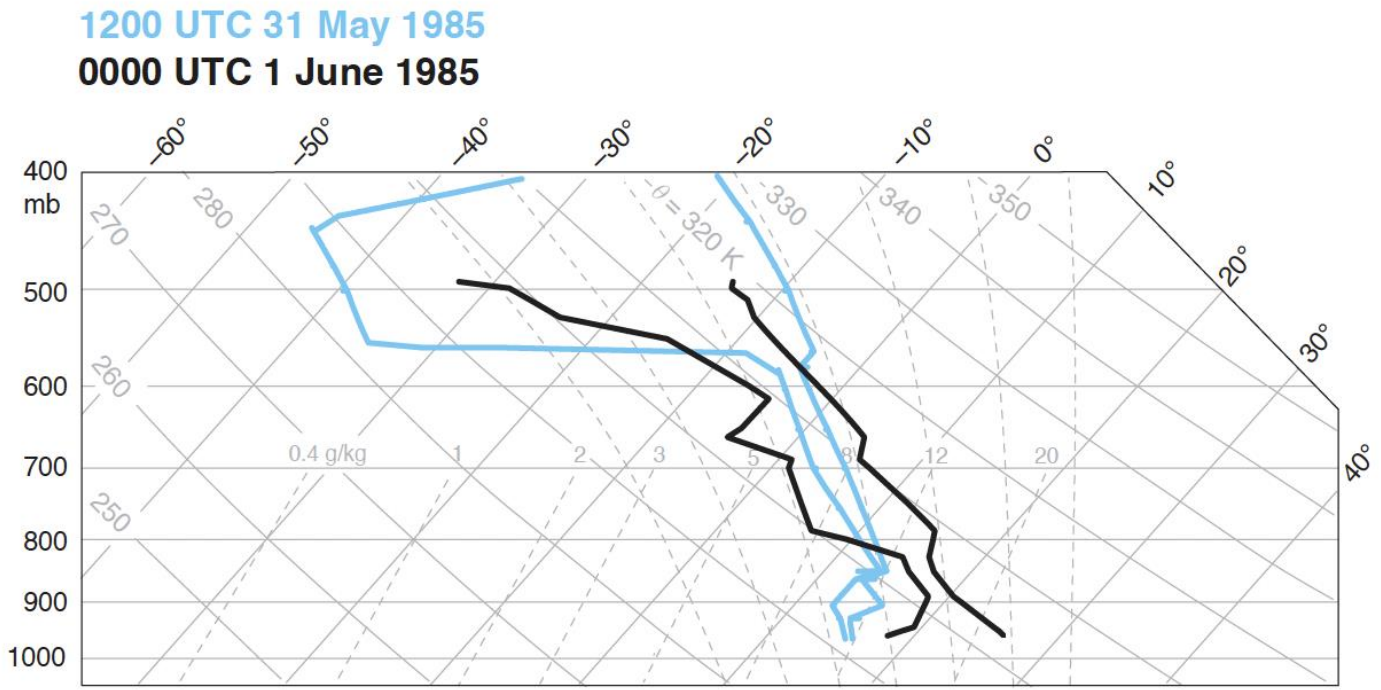

Figure 7.3 Soundings from Pittsburgh, PA, at 1200 UTC 31 May 1985 (blue) and 0000 UTC 1 June 1985 (black). Between 1200 and 0000 UTC, the mean tropospheric lapse rate has undergone significant changes, probably as the result of a number of large-scale processes acting in unison (e.g., insolation, lapse rate advection/differential temperature advection, stretching effect, etc.). The low-level moisture also increased by several g kg^{-1} during the same 12 h period, primarily as a result of moisture advection. The increase in lapse rate and low-level moisture between 1200 and 0000 UTC led to the development of large CAPE (the lifted index decreased from +3 to −7; the lifted index is the temperature difference between the environmental 500 mb temperature and the temperature of an air parcel that has been lifted to 500 mb from the surface, with negative indices indicating that the lifted parcel is warmer than the environment at 500 mb). (Large vertical wind shear also accompanied the large instability; the worst tornado outbreak in the history of Pennsylvania was in progress not far from Pittsburgh at 0000 UTC.)

水平平流作用 $-\vec{\mathbf{v}}_{\mathrm{h}} \cdot \nabla_{\mathrm{h}} \gamma$

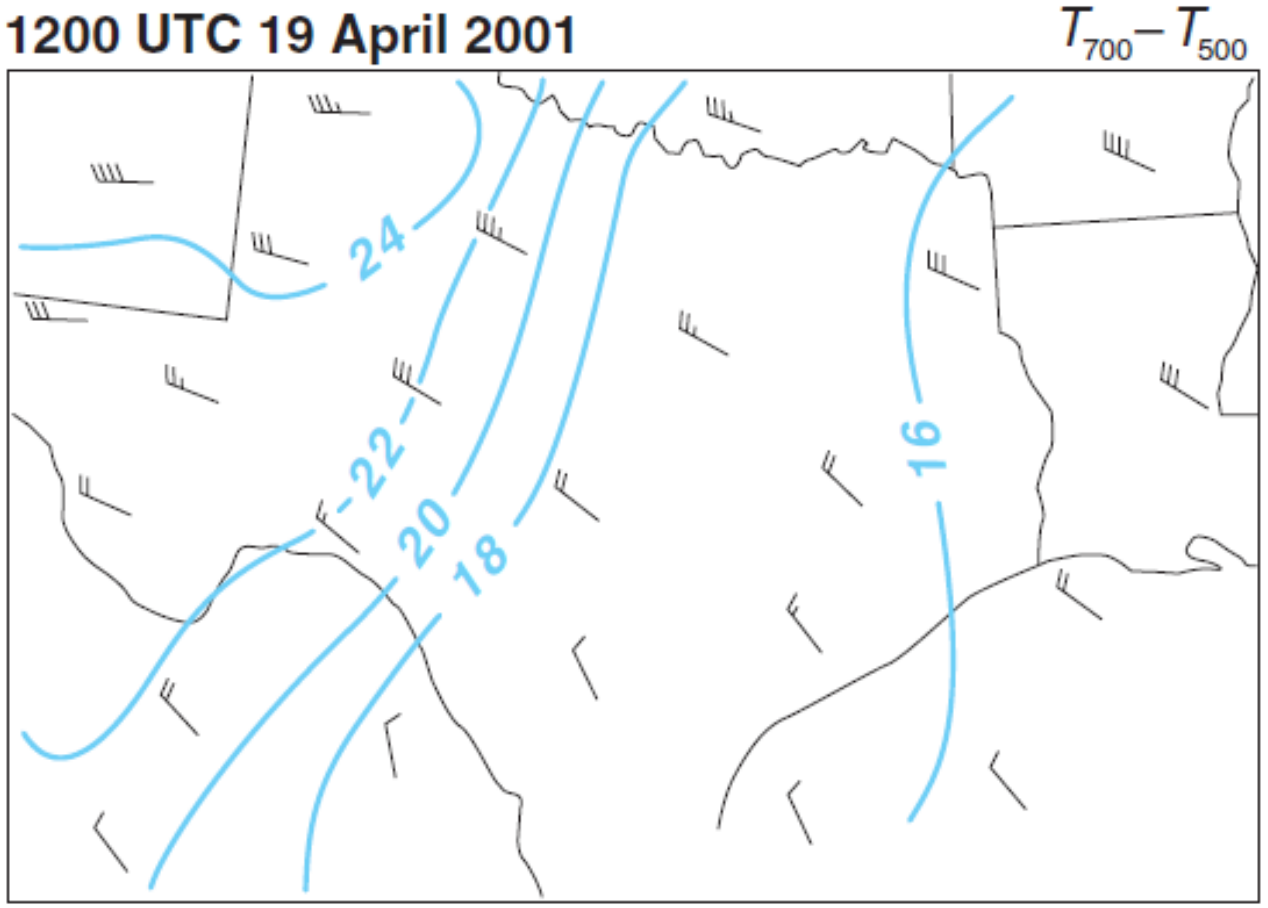

Figure 7.4 Analysis of the environmental temperature difference between 500 and 700 mb (K), which is a bulk measure of the midlevel lapse rate (a temperature difference of 27 K between 500 and 700 mb corresponds to an approximately dry adiabatic environmental temperature profile), revealing the presence of horizontal lapse rate advection. Wind barbs depict the mean wind in the 500–700 mb layer. Large lapse rates from the high terrain of northern Mexico and eastern New Mexico are being advected toward the southern Great Plains of the United States. This common warm season phenomenon leads to the formation of the elevated mixed layer that caps soundings in the Great Plains region.

垂直平流作用$w\frac{\partial \gamma}{\partial z}$

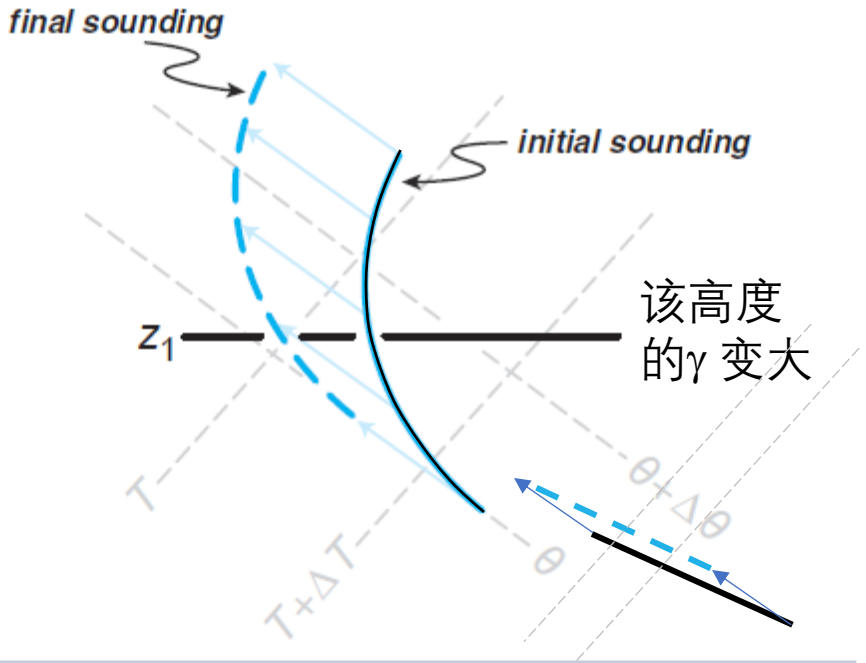

Assume

- w >0, and is constant.
- Adiabatic process
- Lapse rate decrease with height initially

Upward lifting cause cooling

- Always happen when $\gamma<\Gamma_d$
- Cooling is more important for cap removal and CI than the decrease of Lapse rate.
  - Decrease of lapse rate may not be quite significant depending on the initial γ , $\partial\gamma/\partial z$, $\partial w/\partial z$.

Figure 7.5 Schematic thermodynamic diagram illustrating the effect of vertical lapse rate advection. The light blue arrows indicate dry adiabatic parcel displacements. At level z_1, $\partial\gamma/\partial z < 0$, so when upward motion is imposed ($w > 0$ but $\partial w/\partial z = 0$, so that all of the parcels are displaced upward by the same distance) larger lapse rates are advected from below z_1 upward to z_1, increasing the lapse rate there. Note that this process occurs adiabatically, so that cooling has occurred at z_1 in addition to increasing the lapse rate there. This cooling associated with upward motion is typically more important for cap removal and thunderstorm initiation than just the increasing lapse rate. For example, dry adiabatic large-scale ascent *always* leads to cooling (and cap weakening) when lapse rates are less than dry adiabatic, but lapse rate changes resulting from large-scale ascent may or may not be significant, depending on the initial γ, $\partial\gamma/\partial z$, and $\partial w/\partial z$.

差分温度平流

$$-\vec{\mathbf{v}_\mathrm{h}}\cdot\nabla_\mathrm{h}\gamma+\frac{\partial\vec{\mathbf{v}_\mathrm{h}}}{\partial z}\cdot\nabla_\mathrm{h}T=-\frac{\partial}{\partial z}(-\vec{\mathbf{v}_\mathrm{h}}\cdot\nabla_\mathrm{h}T)$$

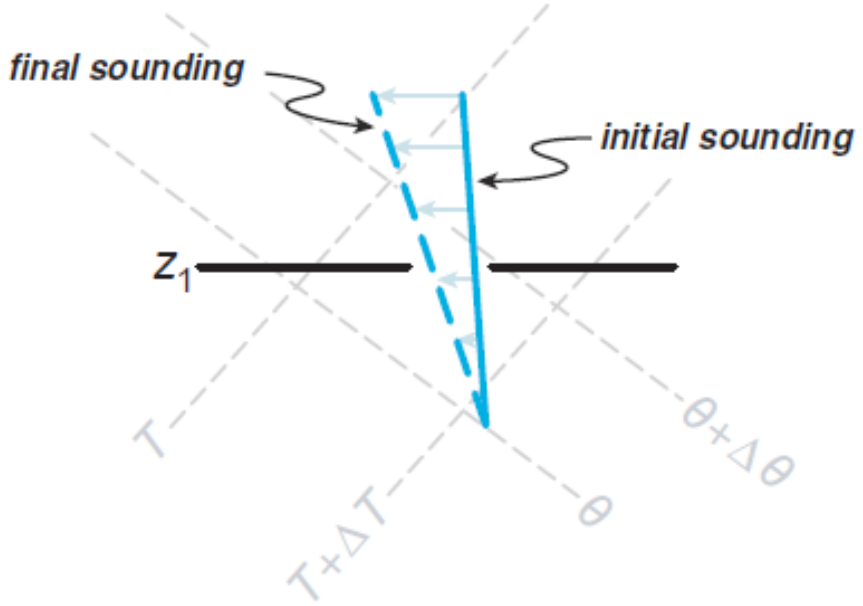

Figure 7.6 Schematic thermodynamic diagram illustrating the effect of differential horizontal temperature advection (by the ageostrophic wind) on the lapse rate (temperature changes are indicated by the light blue arrows). Cold advection increases with height at level z_1, which leads to an increase in the lapse rate at that level. This effect is really the same effect as illustrated in Figure 7.4.

拉伸项

$$\frac{\partial w}{\partial z}(\Gamma_{\mathrm{d}} - \gamma)$$

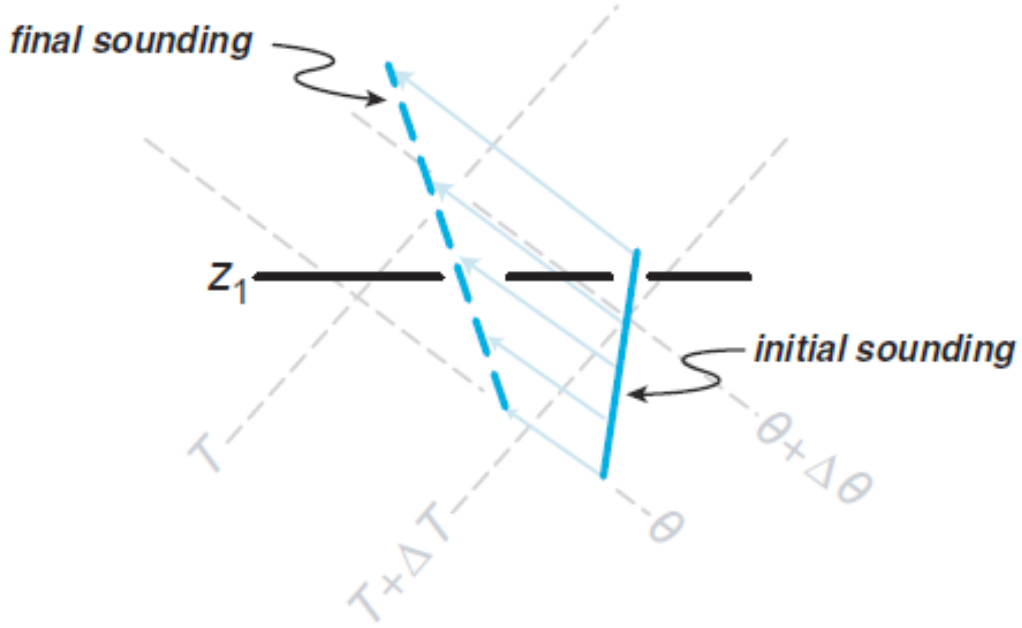

Figure 7.7 Schematic thermodynamic diagram illustrating the stretching effect on lapse rate. In this example, $\Gamma_{\mathrm{d}} > \gamma$ and $\partial w/\partial z > 0$, therefore the lapse rate at level z_1 increases in time. The light blue arrows indicate dry adiabatic upward parcel displacements (because $\partial w/\partial z > 0$, the displacements increase with height).

差分非绝热加热

$$-\frac{1}{c_p}\frac{\partial q}{\partial z}$$

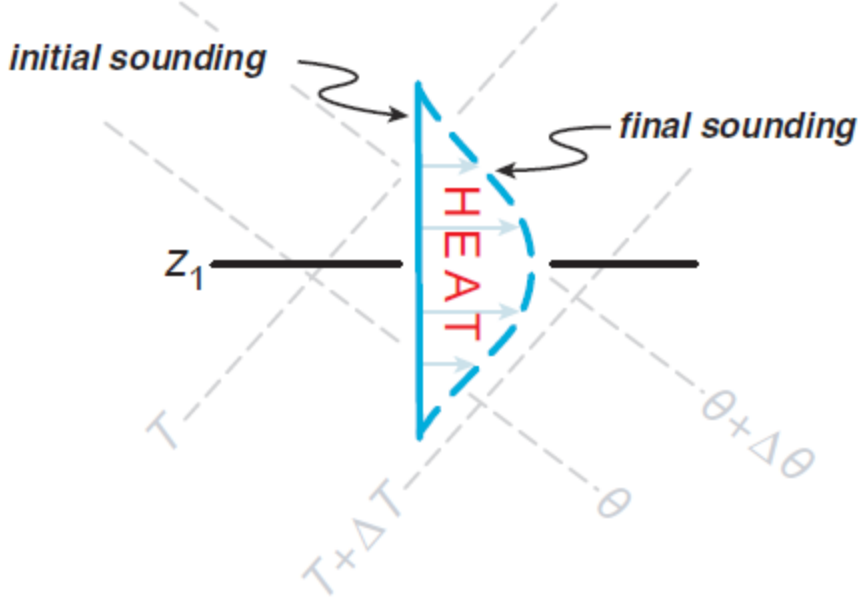

Figure 7.8 Schematic thermodynamic diagram illustrating the effects of differential diabatic heating on lapse rate (temperature changes are indicated by the light blue arrows). The maximum latent heating occurs at level z_1, where $\partial q/\partial z = 0$ and the lapse rate is unchanged. The lapse rate increases above the level of maximum heating ($z > z_1$) and decreases below the level of maximum heating ($z < z_1$).

2）与$\frac{\partial \gamma}{\partial t}$无关的改变CAPE和CIN的过程

上述Lapse rate的变化分析多为对中层Lapse rate的改变，可能会过分强调γ变化对CAPE和CIN变化的作用

- **large-scale rising motion**
- **Moistening**
- **low-level warming**

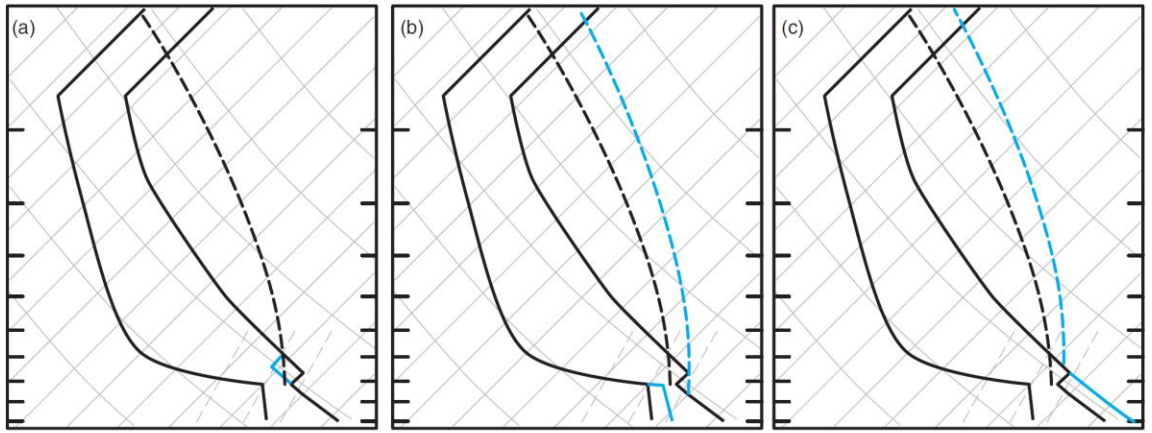

Figure 7.9 CIN can be reduced by (a) large-scale rising motion, (b) low-level moistening (e.g., moisture advection), and (c) low-level warming (e.g., insolation), despite the fact that the CIN modifications may not be accompanied by lapse rate changes, at least not over a significant depth. In (a)–(c), the isotherms and isentropes are solid gray lines, the constant mixing ratio lines are gray dashed lines, the sounding and trajectory taken by an air parcel lifted from the surface are solid and dashed black curves, respectively, and the modified sounding and parcel trajectory are blue solid and dashed curves, respectively. In (a), for clarity, only the temperature profile has been modified (the moisture profile has not been modified in accordance with the vertical motion that has been imposed in the layer of the capping inversion). Note that (b) and (c) are also accompanied by increases in CAPE. Conversely, CIN is augmented by large-scale descent, boundary layer cooling (although this would typically not occur without a concurrent stabilization of the lapse rate), and boundary layer drying (not shown).

(2）中尺度系统的作用

1） 热力场的不均匀性

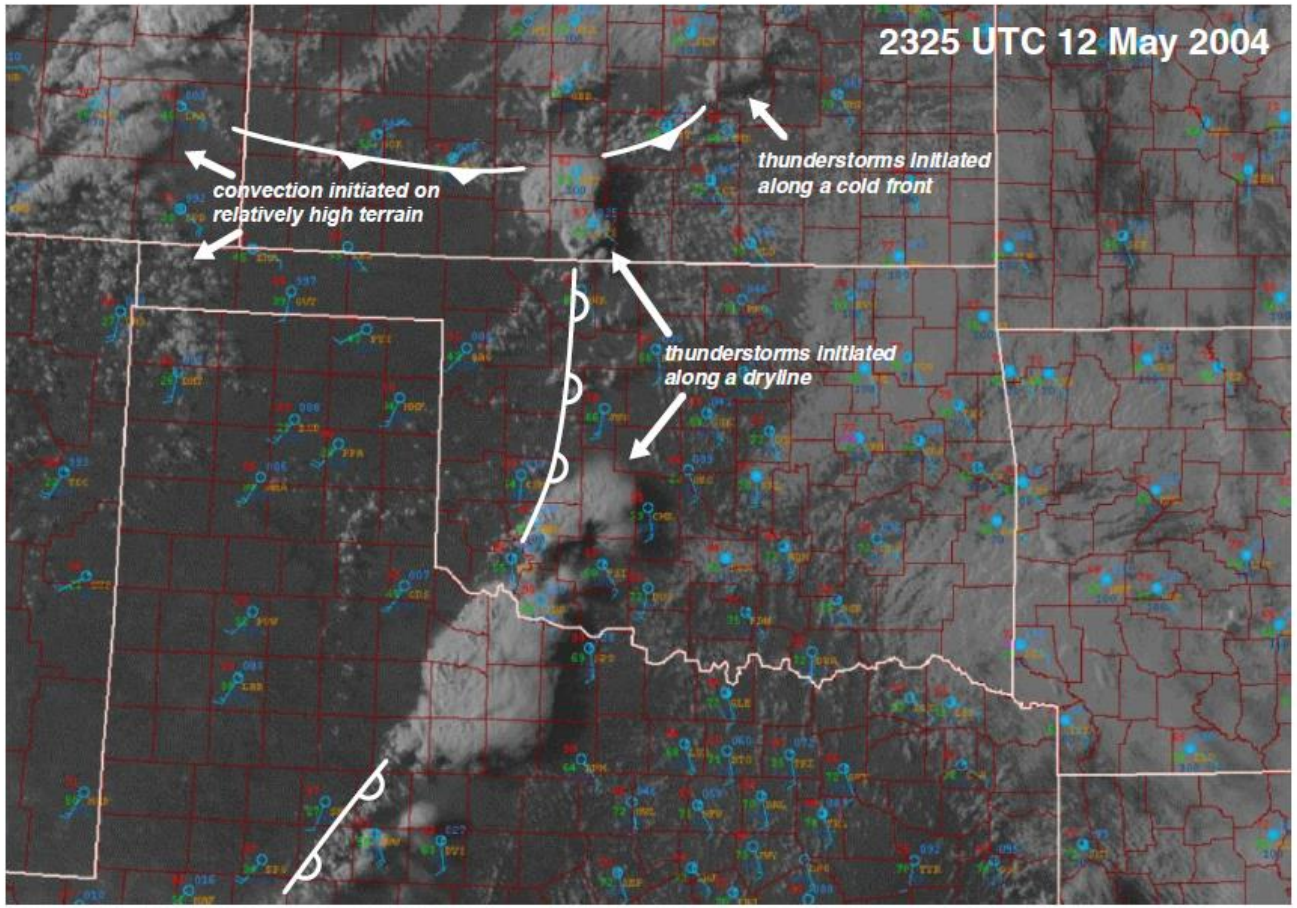

DMC仅在边界的某些部分发生

2）中尺度运动特征（动量）的不均匀性

Convective rolls

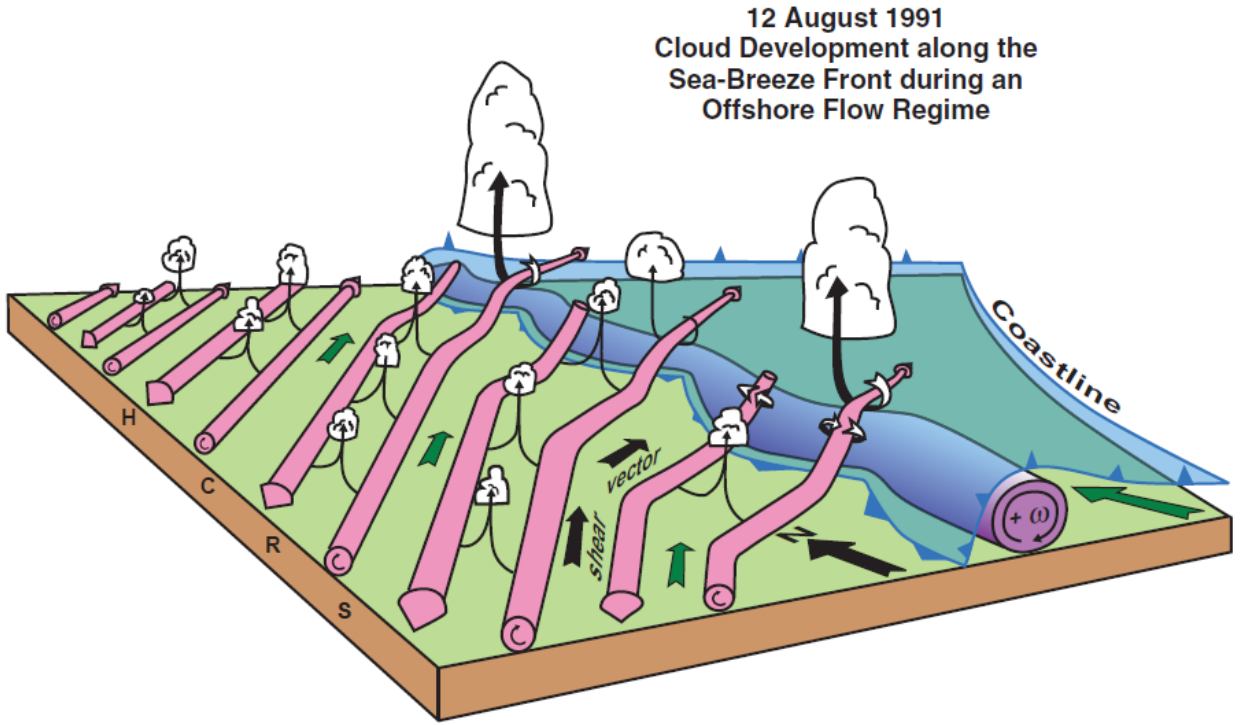

Figure 7.11 Schematic diagram showing the interaction between the sea-breeze front and horizontal convective rolls and how it related to cloud development on 12 August 1991 during the Convection and Precipitation/Electrification Experiment (CaPE). The sea-breeze front is delineated by the heavy blue barbed line. The circulation along the leading portion of the sea-breeze front is shaded purple. The horizontal vorticity vectors associated with the counter-rotating roll circulations are also shown, as are clouds along the horizontal convective rolls and at the intersection points along the front. The shear vector and low-level winds are indicated with black and green arrows, respectively. This is the same case as shown in Figure 5.33. (Adapted from Atkins and Wakimoto [1995].)

Convective rolls

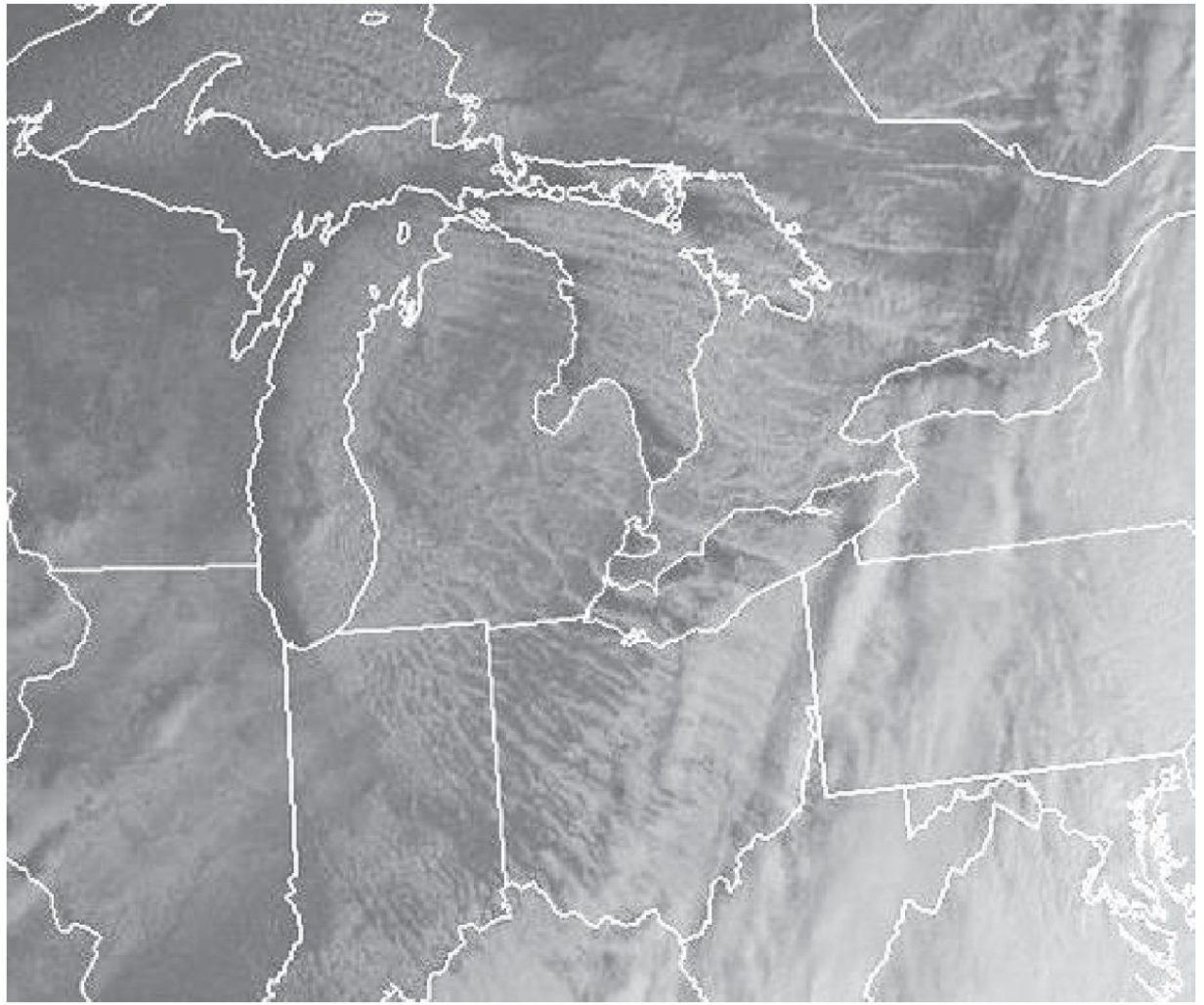

Figure 4.13 HCRs observed in the wake of a cold front in the United States Great Lakes region at 1415 UTC 14 January 2005.

Convective rolls

Figure 4.14 Cloud streets (a manifestation of HCRs) viewed from an airplane. Photograph by Joel Gratz.

Convective rolls

Vertical: Boundary layer depth
Aspect ration: 3-10
Orientation: 30 degree of the mean wind in the boundary layer

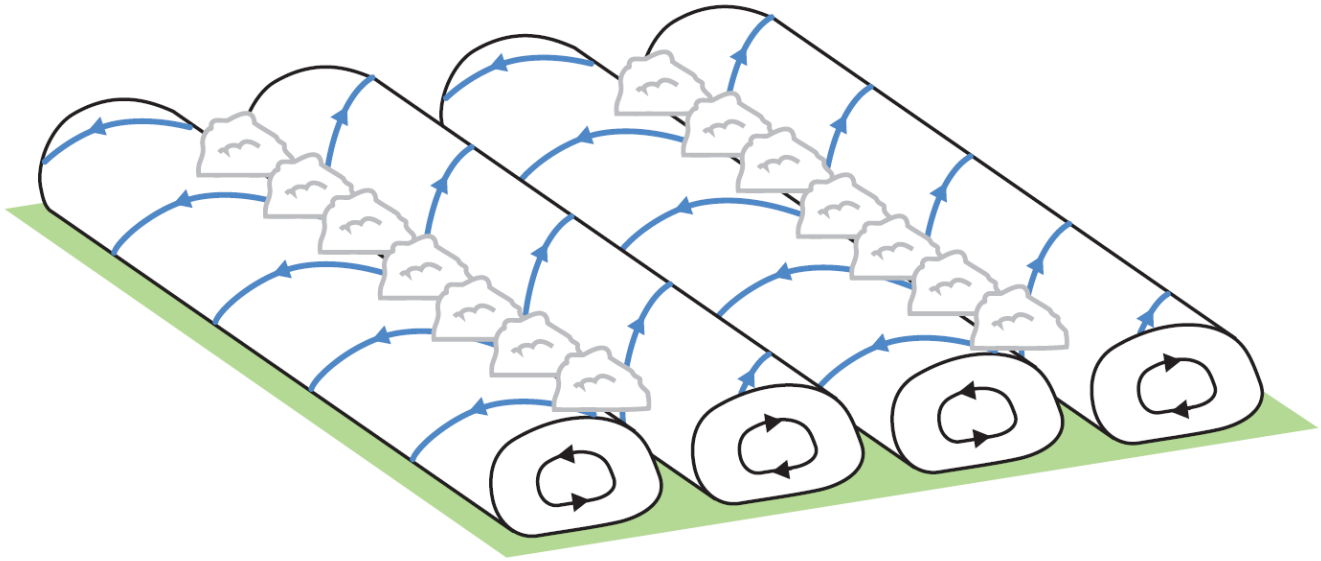

Figure 4.15 Schematic illustration of HCRs in the boundary layer. Black arrows indicate the winds due to the rolls and blue arrows indicate the total wind. Note that the characteristic distance between cloud rows is twice the characteristic width of the convective rolls. (Adapted from Brown [1983].)

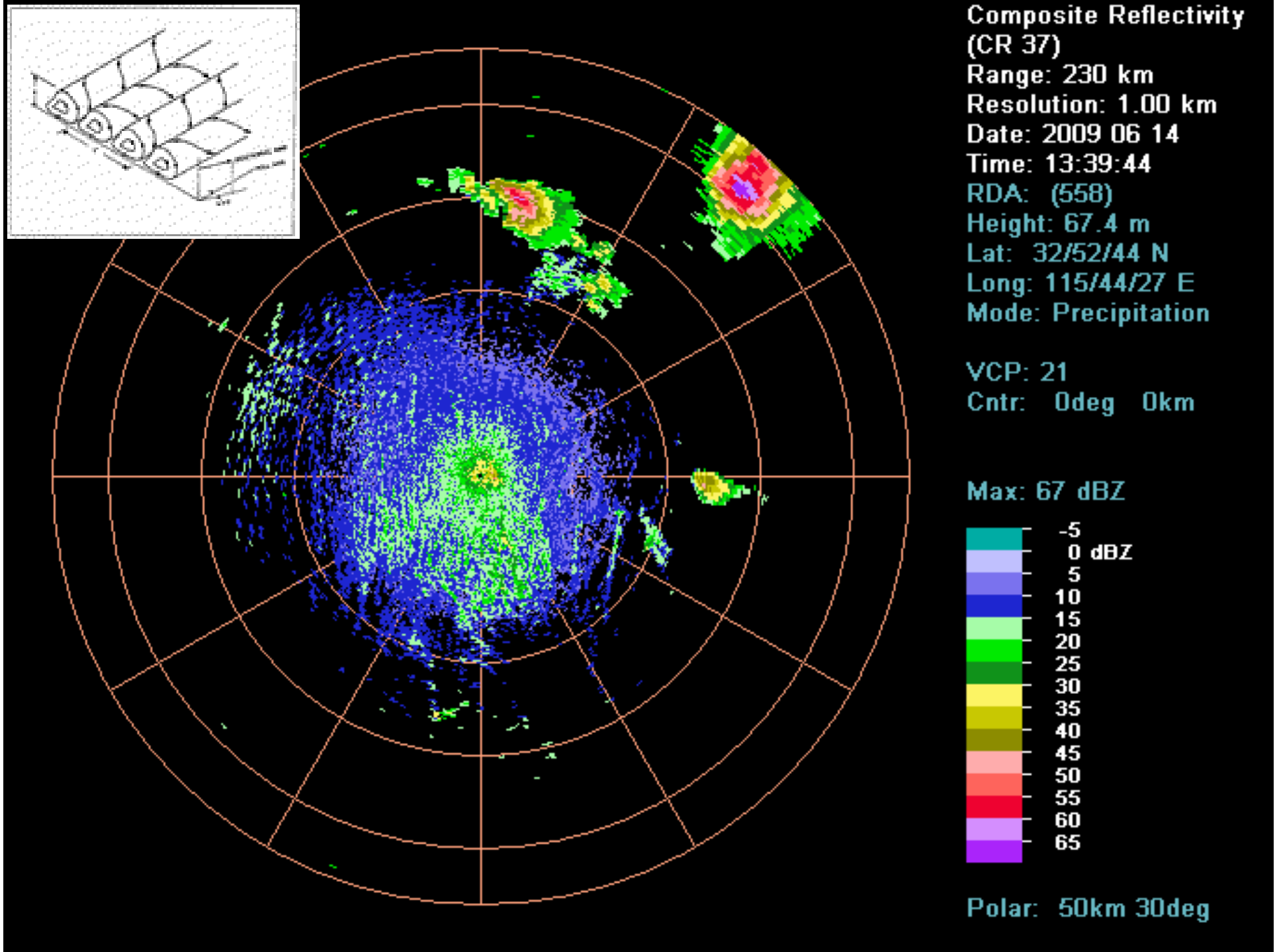
Composite Reflectivity
(CR 37)
Range: 230 km
Resolution: 1.00 km
Date: 2009 06 14
Time: 13:39:44
RDA: (558)
Height: 67.4 m
Lat: 32/52/44 N
Long: 115/44/27 E
Mode: Precipitation
VCP: 21
Cntr: 0deg 0km
Max: 67 dBZ
-5
0 dBZ
5
10
15
20
25
30
35
40
45
50
55
60
65
Polar: 50km 30deg

2）中尺度运动特征（动量）的不均匀性

Misocyclone

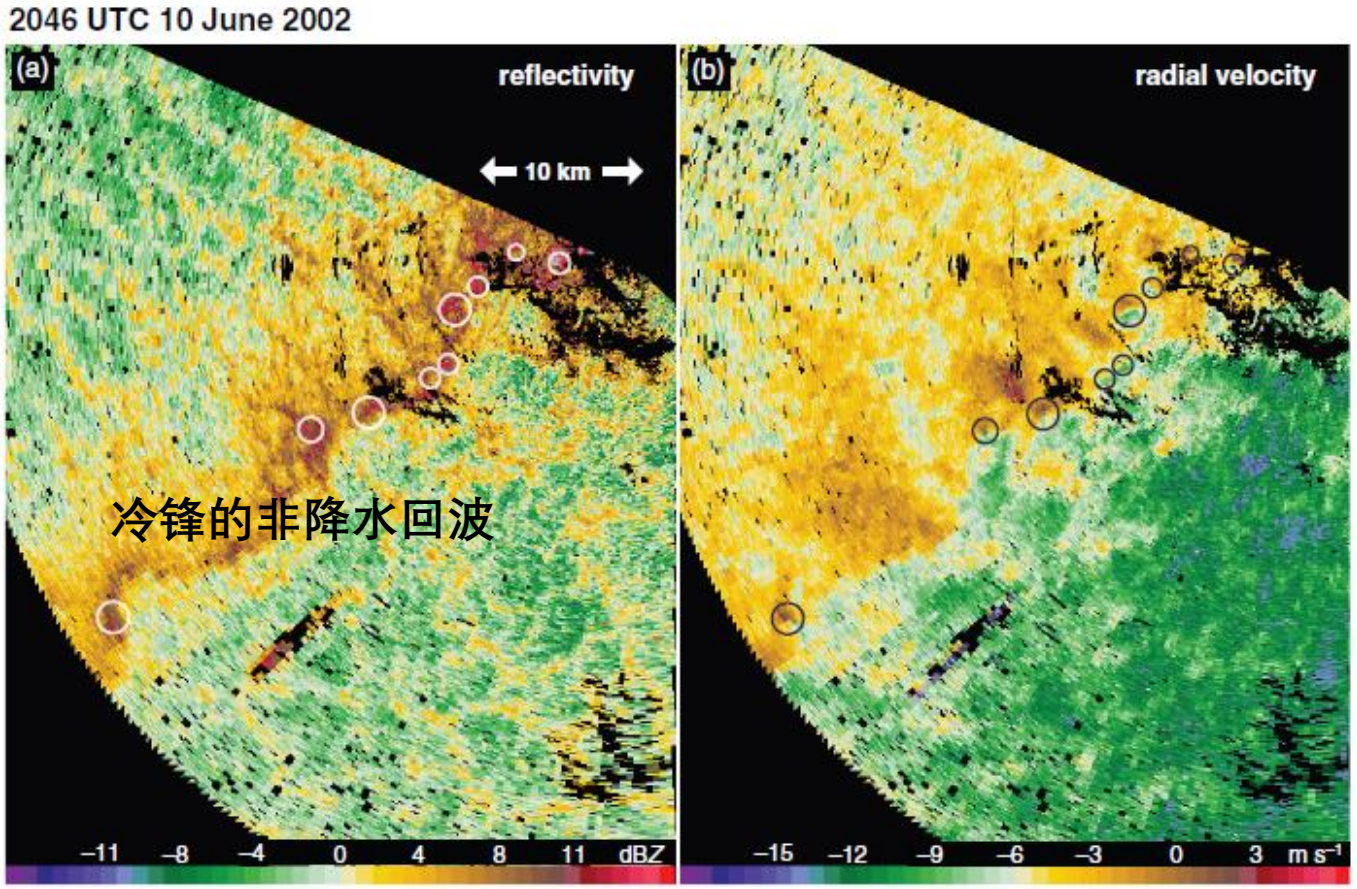

晴空模式

Figure 7.12 Misocyclones (circled) along a non-precipitating cold front evident in (a) reflectivity (dBZ; reflectivity values are uncalibrated) and (b) radial velocity (m s^{-1}) data obtained by the Doppler On Wheels (DOW) radar in western Kansas on 10 June 2002 (0.5° elevation angle). The reflectivity is mainly attributable to insects. Horizontal shear instability likely played a role in the formation of the vortices.

2）中尺度运动特征（动量）的不均匀性

Misocyclone

- Convergence increases between misocyclones
- Impact of the size of misocyclone
- Interaction between misocyclones

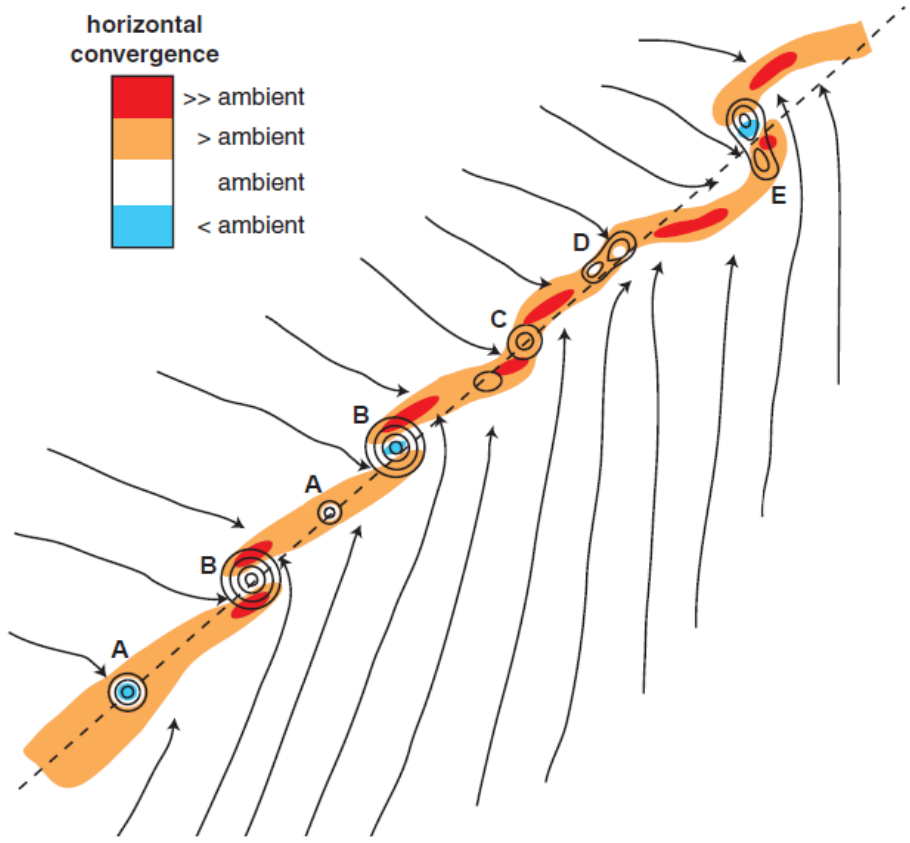

Figure 7.13 Conceptual model of misocyclones (vertical vorticity, ζ, greater than the ambient value is contoured), horizontal convergence (shaded), and streamlines based on a sample of air mass boundaries observed during the International H_2O Project (IHOP), one of which was the case shown in Figure 7.12. The misocyclones at both A positions are small relative to the average width of the mesoscale convergence zone. The misocyclones at both B positions are large compared with the width of mesoscale convergence zone. The misocyclone at position C has a width similar to that of the convergence zone. Merging misocyclones aligned with the boundary and oriented perpendicular to the boundary are located at positions D and E, respectively. (From Marquis *et al.* [2007].)

(3）DMC触发预报的误差分析

- 完全没有CIN，DMC不发展
- 有很大的CIN，DMC仍发展
- 有CAPE，skew-T 估计的CIN被overcome (比如地面升温到了对流温度），但没有对流发展。

1） 探空的代表性

位置、对流污染

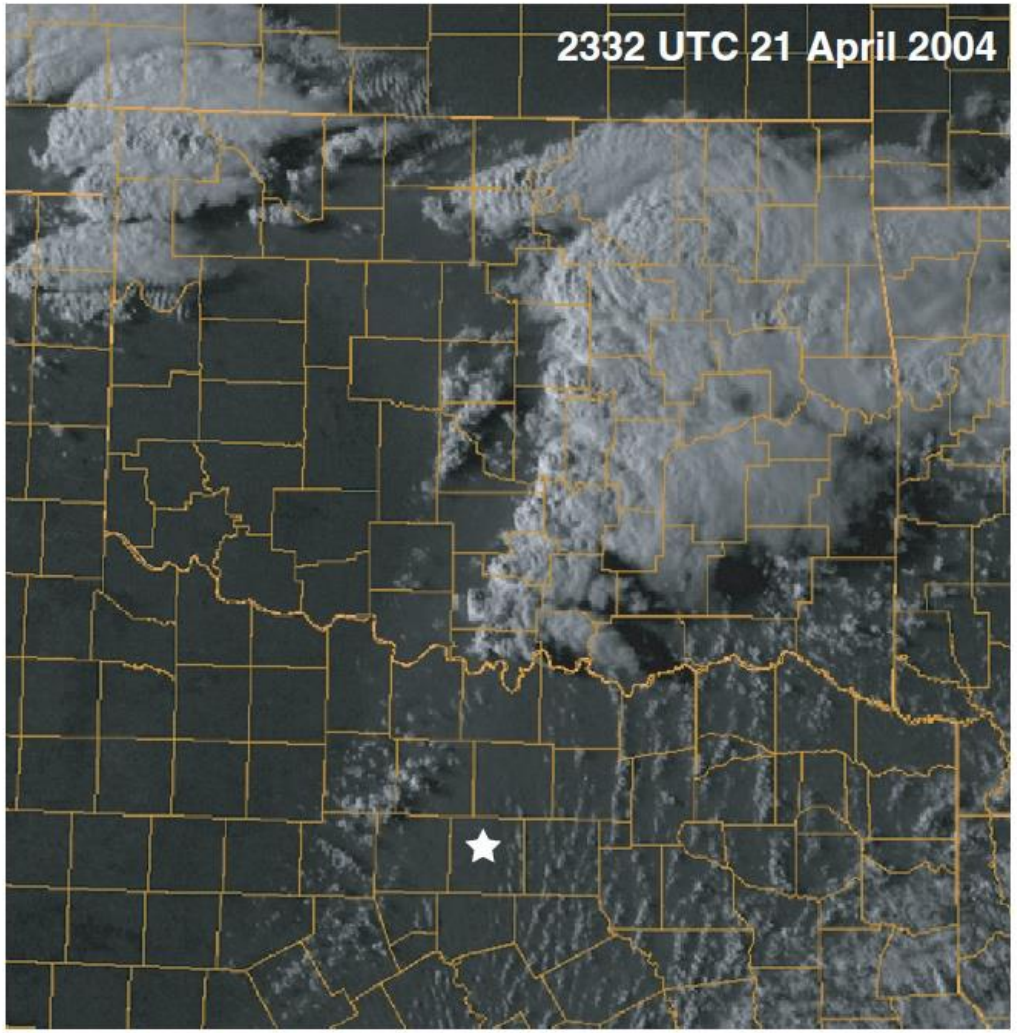

1） 探空的代表性

PBL roll 的影响

Sounding in downdraft overestimates the LCL

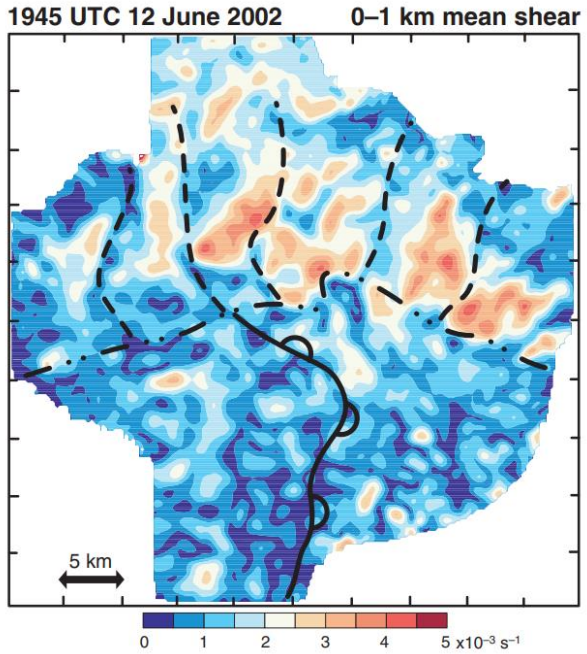

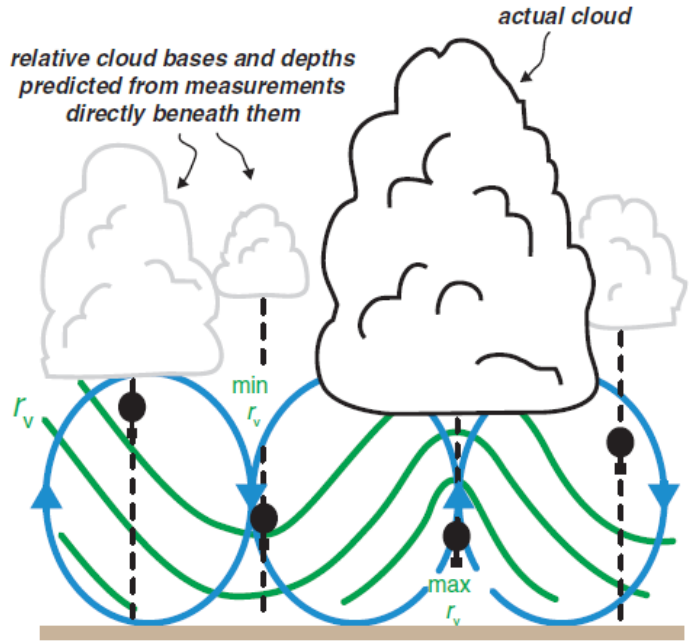

Figure 7.16 Schematic showing the effect of boundary layer roll circulations on the moisture profiles measured by soundings. A sounding that ascends through the updraft of a roll samples larger water vapor concentrations than a sounding that ascends through the downdraft of a roll. Thus, the LCL height based on a sounding that has ascended through a downdraft might be overestimated compared with the bases of the observed clouds, which generally reside within boundary layer updrafts. CAPE and CIN values computed from a sounding would also be sensitive to whether the sounding ascended through an updraft or a downdraft. (Adapted from Weckwerth *et al.* [1996].)

2） CIN没有被完全overcome

Skew-T估计的CIN比实际偏低

有CAPE，skew-T 估计的CIN被overcome (比如地面升温到了对流温度），但没有对流发展。

气块的初始来源

气块从地面抬升的话，w, θ 在干绝热过程中从地面到LCL保守，忽略了干空气混合，导致LCL， LFC偏低，CIN偏小。

解决办法：气块从距离地面50-100 hPa的平均值（或PBL整层平均）开始抬升。

湿环境比较有利于CIN的准确估计。

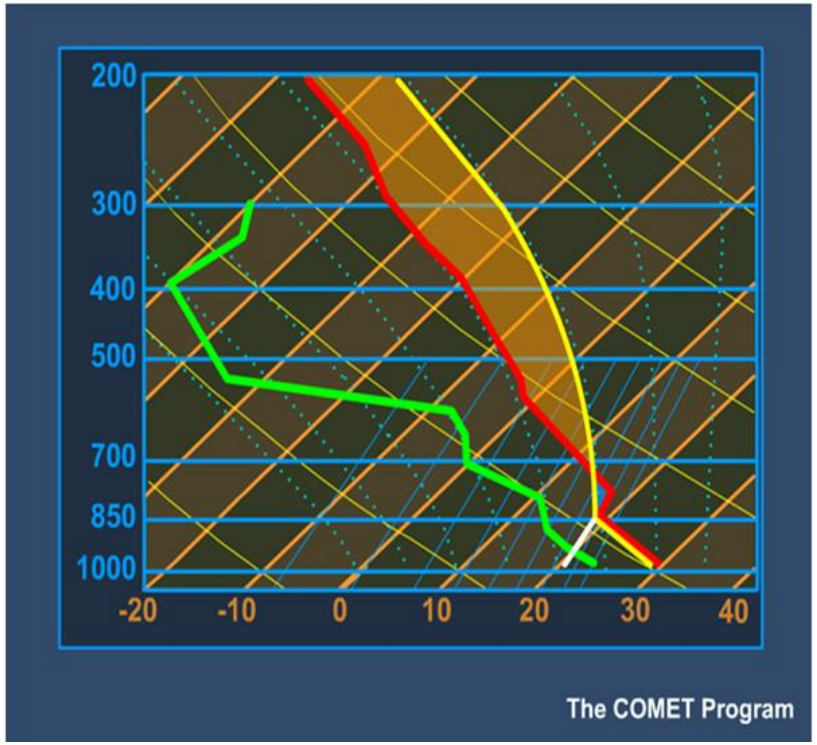

例子：探空处CIN为0，DMC没发展

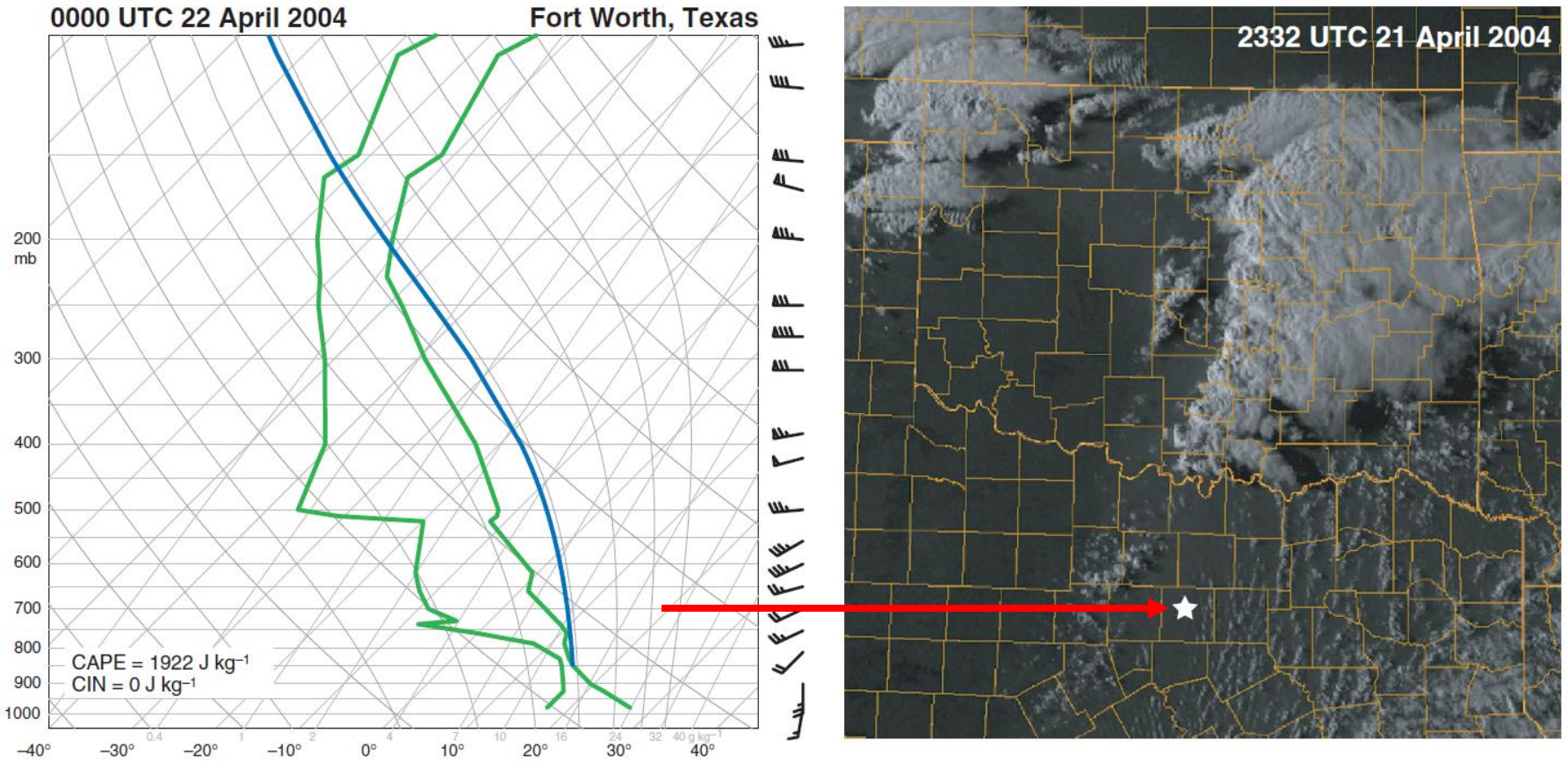

Figure 7.15 Example of convection initiation 'failure' in the absence of CIN on 21 April 2004. The Fort Worth, TX, sounding (left) has no CIN and appreciable CAPE, yet the only thunderstorms that developed were over 150 km north of the 0000 UTC sounding location, indicated by the star in the 2332 UTC visible satellite image (right). The CIN is zero, even neglecting virtual temperature effects.

Skew-T估计的CIN比实际偏低

CIN：蓝色阴影

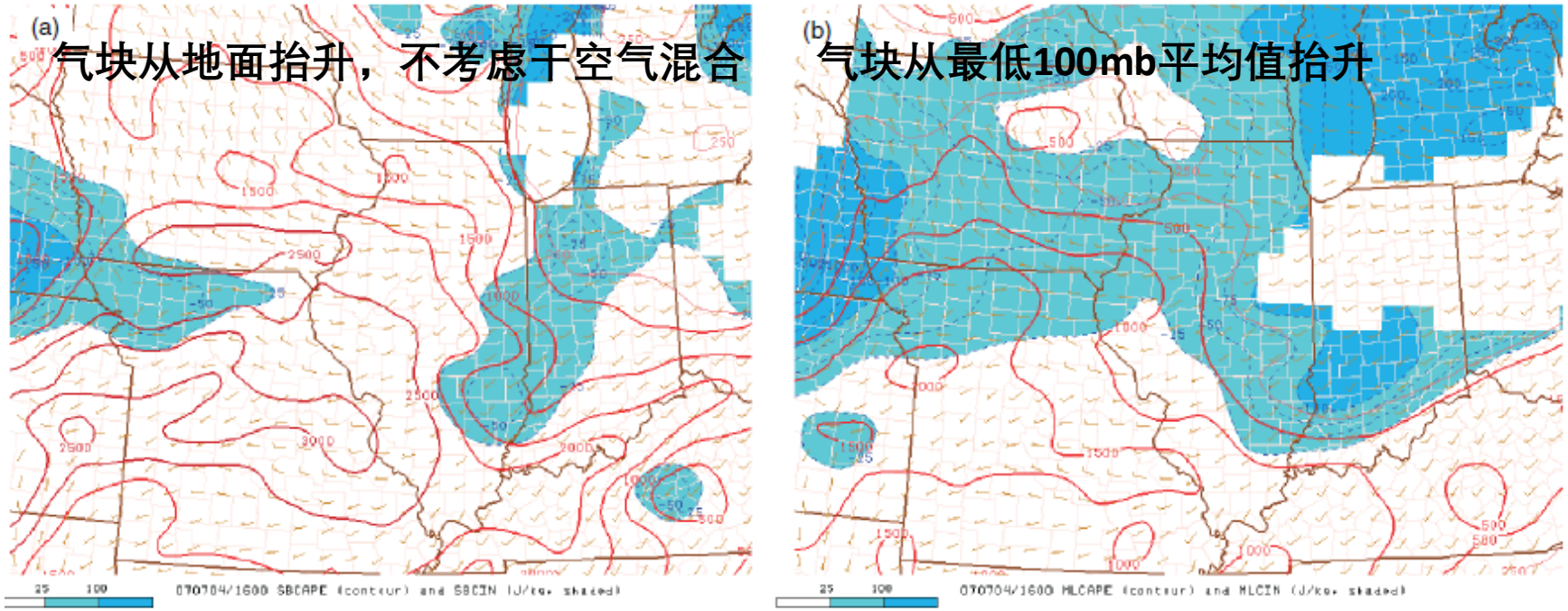

Figure 7.18 Comparison of CAPE (red contours; J kg^{-1}) and CIN values (blue shading; J kg^{-1}) computed by lifting (a) a parcel from the surface, assuming no mixing, and (b) a parcel having the mean potential temperature and water vapor mixing ratio of the lowest 100 mb, which crudely attempts to account for mixing that occurs en route to the LFC. CAPE (CIN) values are typically smaller (larger) when a parcel is lifted having the mean properties of the lowest 100 mb (or some layer of roughly similar depth), as is the case above, except perhaps at night or on the cold side of a front, where a shallow layer of relatively cool air might be found near the surface. (Courtesy of the Storm Prediction Center.)

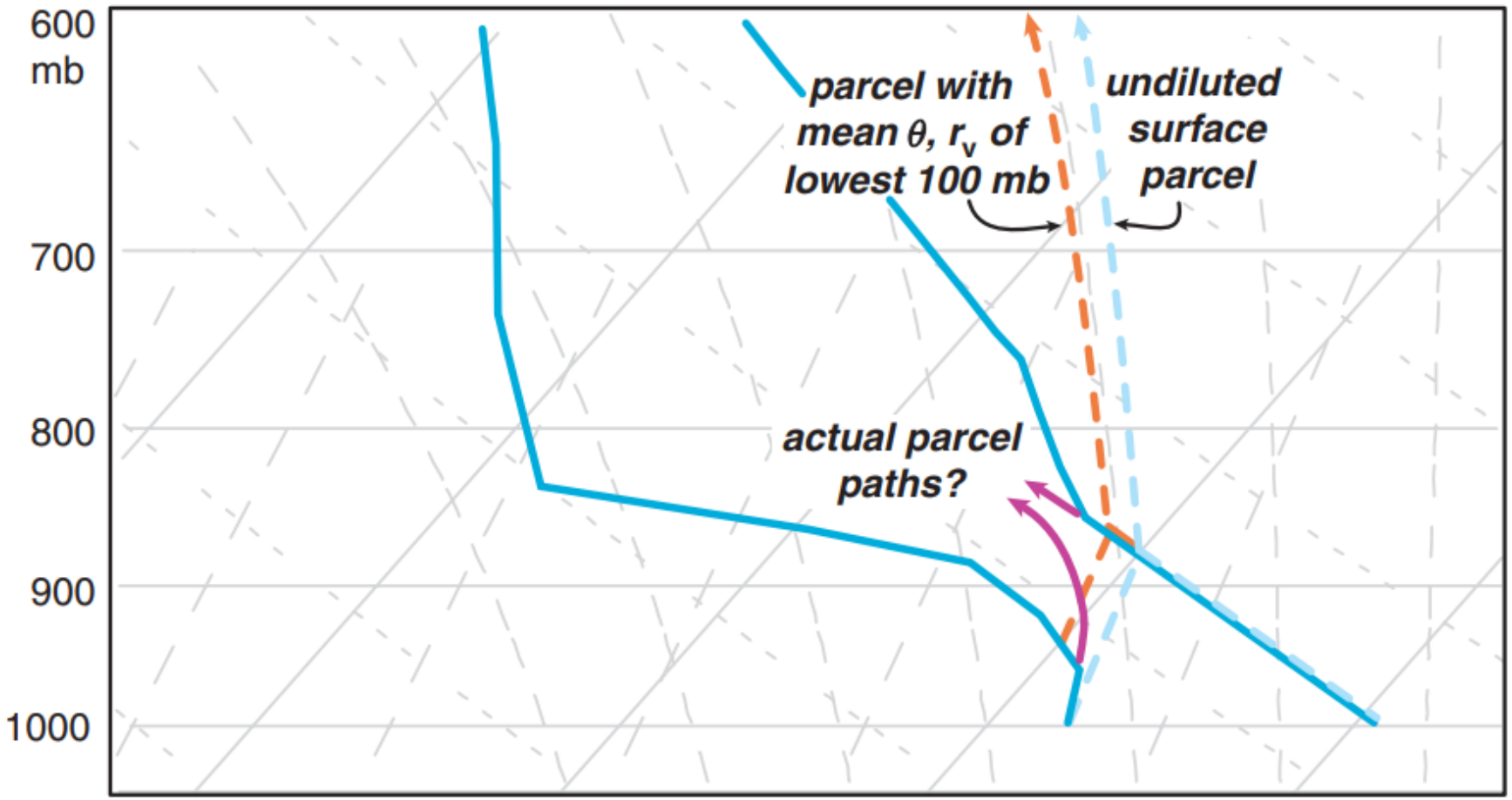

Fig. 7.19 adapted from MR2010

Entrainment rate is large for large vertical wind shear environment

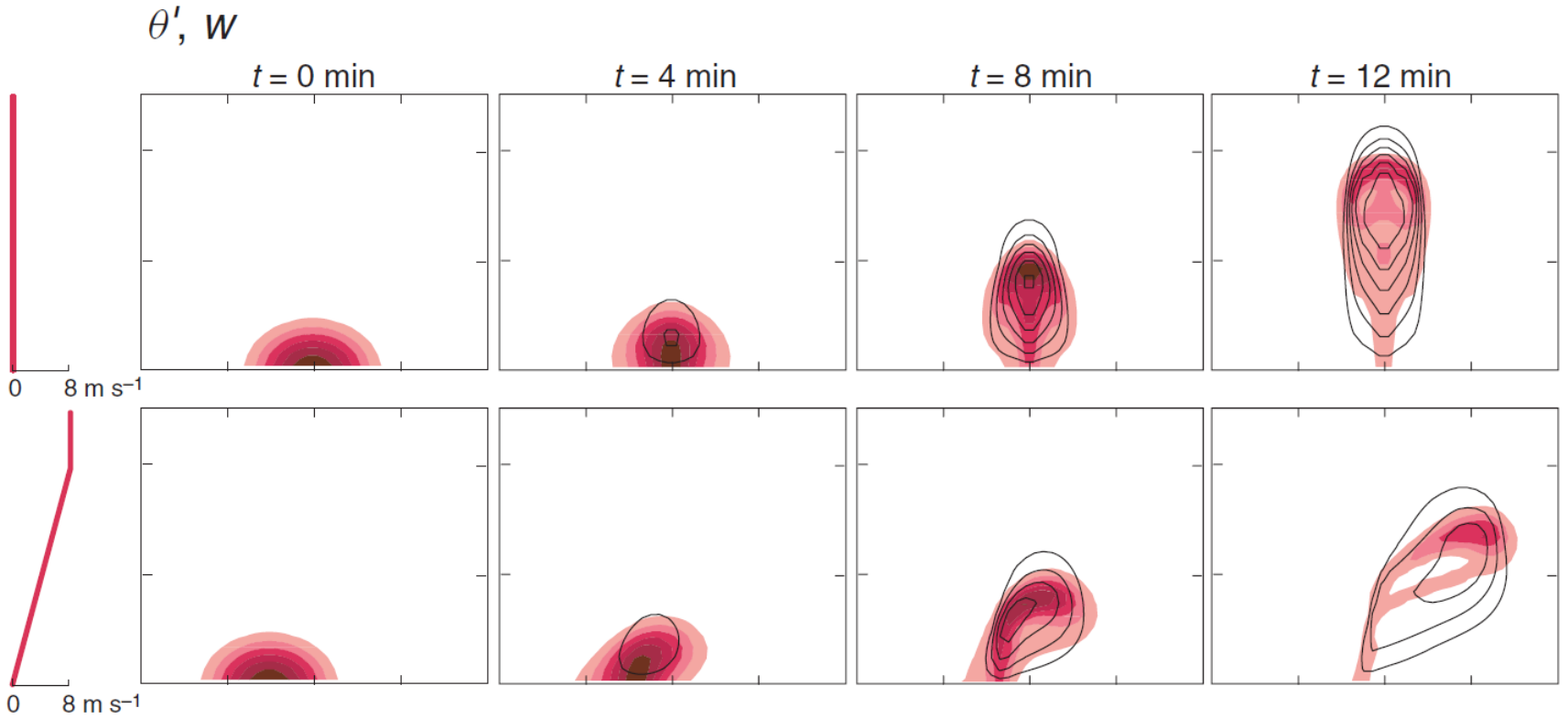

Entrainment rate is large for large vertical wind shear environment

（4）有利于DMC发生的条件

持续的低层辐合和较小的CIN

水汽的辐合：如何有利于CI的发生？

在持续性辐合的气团边界往往观测到较大的水汽混合比q_v

水汽的辐合能被解释为制造水汽混合比q_v的极值吗？

1) 水汽的水辐合本身并不能形成局地 q_v极大值

$$-\nabla\cdot(q_v\,\vec{\mathrm{v}}_\mathrm{h})>0$$

$$\frac{\partial q_v}{\partial t}=-\vec{\mathrm{v}}\cdot\nabla q_v-\mathrm{C}+\mathrm{E}=-\vec{\mathrm{v}}_\mathrm{h}\cdot\nabla_\mathrm{h}q_v-w\frac{\partial q_v}{\partial z}-\mathrm{C}+\mathrm{E}\quad①$$

Boussinesq近似： $\nabla_\mathrm{h}\cdot\vec{\mathrm{v}}_\mathrm{h}+\frac{\partial w}{\partial z}=0$

（4）有利于DMC发生的条件

持续的低层辐合和较小的CIN

水汽的辐合：如何有利于CI的发生？

在持续性辐合的气团边界往往观测到较大的水汽混合比q_v

水汽的辐合能被解释为制造水汽混合比q_v的极值吗？

1) 水汽的水辐合本身并不能形成局地 q_v极大值

$$-\nabla\cdot(q_v\,\vec{\mathrm{v}}_\mathrm{h})>0$$

$$\frac{\partial q_v}{\partial t}=-\vec{\mathrm{v}}\cdot\nabla q_v-\mathrm{C}+\mathrm{E}=-\vec{\mathrm{v}}_\mathrm{h}\cdot\nabla_\mathrm{h}q_v-w\frac{\partial q_v}{\partial z}-\mathrm{C}+\mathrm{E}\quad①$$

在不考虑蒸发的情形下， 水汽的增加只能来自平流，而平流并不能产生局地极大值

Boussinesq近似：

$$\frac{\partial q_v}{\partial t} = -\vec{\mathrm{v}}_\mathrm{h} \cdot \nabla_\mathrm{h} q_v - w\frac{\partial q_v}{\partial z} - \mathrm{C} + \mathrm{E} \quad ①$$

$$\nabla_\mathrm{h} \cdot \vec{\mathrm{v}}_\mathrm{h} + \frac{\partial w}{\partial z} = 0 \qquad q_v \nabla_\mathrm{h} \cdot \vec{\mathrm{v}}_\mathrm{h} + q_v \frac{\partial w}{\partial z} = 0 \quad ②$$

① + ② $\Rightarrow$

$$\frac{\partial q_v}{\partial t} = -\vec{\mathrm{v}}_\mathrm{h} \cdot \nabla_\mathrm{h} q_v - w\frac{\partial q_v}{\partial z} - \mathrm{C} + \mathrm{E}$$

$$-q_v \nabla_\mathrm{h} \cdot \vec{\mathrm{v}}_\mathrm{h} - q_v \frac{\partial w}{\partial z}$$

$$= -\nabla_\mathrm{h} \cdot (q_v \vec{\mathrm{v}}_\mathrm{h}) - \frac{\partial q_v w}{\partial z} - \mathrm{C} + \mathrm{E}$$

若水汽水平辐合 $-\nabla_\mathrm{h} \cdot (q_v \vec{\mathrm{v}}_\mathrm{h}) > 0$, 则 $\frac{\partial q_v}{\partial t} > 0$

如果 $-\nabla_\mathrm{h} \cdot (q_v \vec{\mathrm{v}}_\mathrm{h}) > 0$, 则有 $-\frac{\partial q_v w}{\partial z} < 0$, 从而 $\frac{\partial q_v}{\partial t} < 0$

$$\frac{\partial q_v}{\partial t} = -\nabla_{\mathrm{h}} \cdot (q_v \vec{\mathrm{v}}_{\mathrm{h}}) - \frac{\partial q_v w}{\partial z} - \mathrm{C} + \mathrm{E}$$

二者的作用抵消后的余项即为水汽的平流作用，而平流并不能产生局地极大值，只能把原来的极大值平流到新的地方。

2) 水汽的辐合会使湿层变厚

$$\nabla_{\mathrm{h}} \cdot (q_v \vec{\mathrm{v}}_{\mathrm{h}}) < 0 \Rightarrow \nabla_{\mathrm{h}} \cdot \vec{\mathrm{v}}_{\mathrm{h}} < 0 \Rightarrow \frac{\partial w}{\partial z} > 0$$

$\Rightarrow$ 边界层的水汽变厚 $\Rightarrow$ 气块的夹卷作用变弱

$\Rightarrow$ 相当位温减小变弱 $\Rightarrow$ CAPE增大

3) 湿层变厚区域，垂直混合对近地面水汽影响不大，而在非辐合区，垂直混合会显著减小近地面的水汽量。因此，垂直混合在水平方向的不均匀性造成地面q_v局地极大值。

Elevated Convection

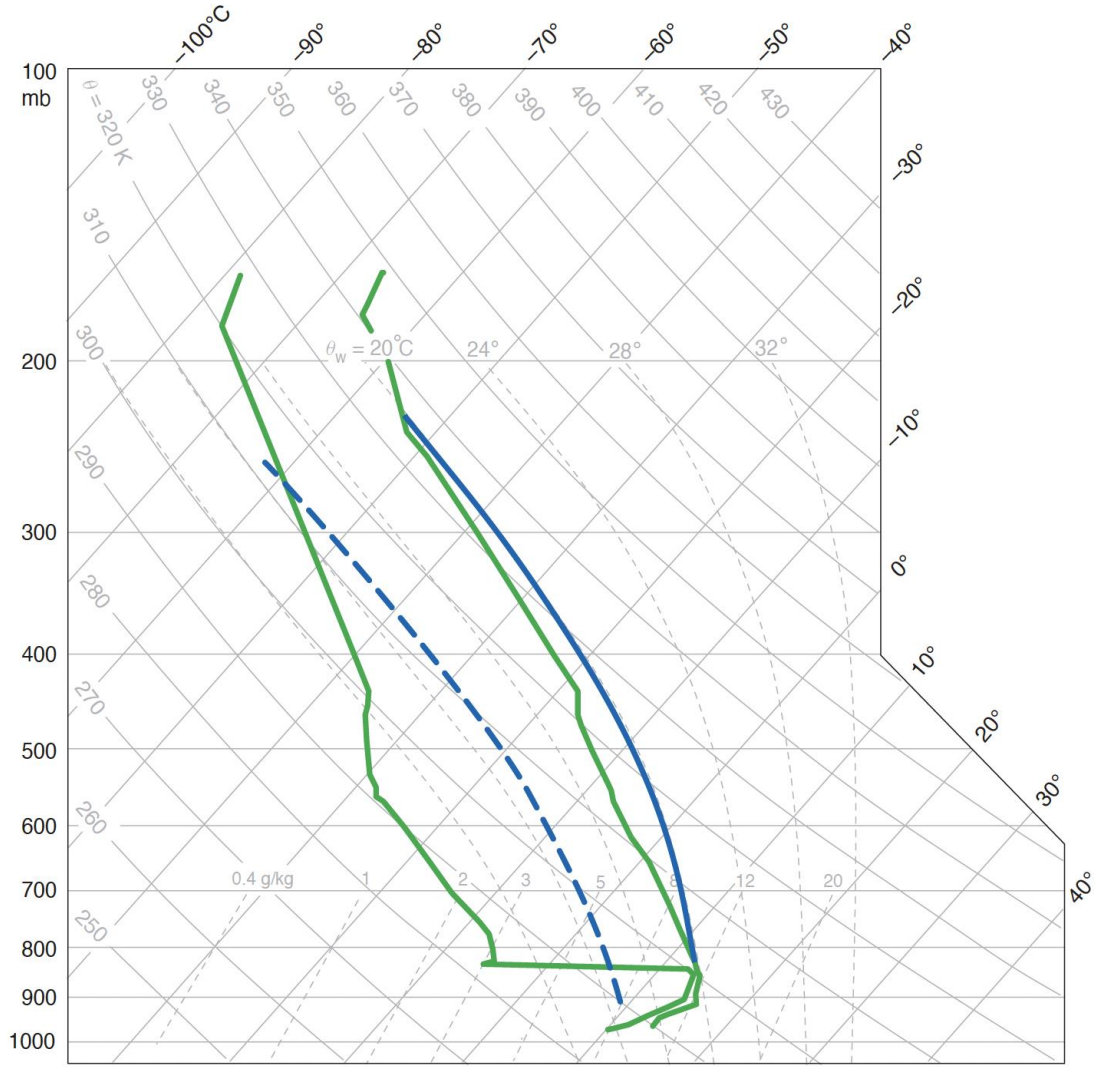

Figure 7.22 Example of a sounding containing elevated CAPE but no surface-based CAPE. A parcel of air lifted from the surface follows the dashed blue trajectory, whereas an air parcel lifted from the top of the stable boundary layer follows the solid blue trajectory.